J. Fluid Mech. (2003), *vol.* 475, *pp.* 377–408.
DOI: 10.1017/S0022112002003014 Printed in the United Kingdom

Marangoni instability of a thin liquid film heated from below by a local heat source

By SERAFIM KALLIADASIS†, ALLA KIYASHKO AND E. A. DEMEKHIN‡

Department of Chemical Engineering, University of Leeds, Leeds LS2 9JT, UK

(Received 3 January 2002 and in revised form 27 June 2002)

We consider the motion of a liquid film falling down a heated planar substrate. Using the integral-boundary-layer approximation of the Navier–Stokes/energy equations and free-surface boundary conditions, it is shown that the problem is governed by two coupled nonlinear partial differential equations for the evolution of the local film height and temperature distribution in time and space. Two-dimensional steady-state solutions of these equations are reported for different values of the governing dimensionless groups. Our computations demonstrate that the free surface develops a bump in the region where the wall temperature gradient is positive. We analyse the linear stability of this bump with respect to disturbances in the spanwise direction. We show that the operator of the linearized system has both a discrete and an essential spectrum. The discrete spectrum bifurcates from resonance poles at certain values of the wavenumber for the disturbances in the transverse direction. The essential spectrum is always stable while part of the discrete spectrum becomes unstable for values of the Marangoni number larger than a critical value. Above this critical Marangoni number the growth rate curve as a function of wavenumber has a finite band of unstable modes which increases as the Marangoni number increases.

1. Introduction

The role of surface tension gradients (Marangoni effect) as a cause of interfacial instabilities has been established by the pioneering studies of Pearson (1958) and Sternling & Scriven (1959). In the context of free-surface thin liquid films, a great deal of theoretical work has been devoted to the effect of surface tension variation on the evolution of the free surface (see for example Oron, Davis & Bankoff 1997 and Davis 1987). The (linear) stability of a planar liquid layer subject to a temperature gradient along the layer has been examined by Smith & Davis (1983*a*, *b*) while Demekhin & Velarde (2001) investigated the linear stability of a falling film with a temperature gradient on the wall. The combined effect of thermocapillary instability and a number of physical factors such as evaporation/condensation, vapour recoil and rupture due to long-range attractive van der Waals interactions has been considered by a number of authors (see for example Burelbach, Bankoff & Davis 1988 and the review paper by Bankoff 1994). Joo, Davis & Bankoff (1991) investigated the thermocapillary instability of a thin liquid film falling down a uniformly heated inclined

† Author to whom correspondence should be addressed: S.Kalliadasis@leeds.ac.uk
‡ Permanent address: Department of Chemical Engineering, University of Notre Dame, Notre Dame, IN 46556, USA.

plane and Oron & Peles (1998) and more recently Oron (1999) examined the stability of a thin non-volatile liquid film in the presence of a spatially uniform heat source within the liquid. A detailed review of interfacial thermocapillary phenomena is given by Nepomnyashchy, Velarde & Colinet (2001).

In this study we consider the thermocapillary Marangoni instability of a thin liquid film heated from below with a local heat source. The motivation arose from the experiments reported recently by Kabov, Marchuk & Chupin (1996), Kabov *et al.* (1999), Kabov (1998) and Scheid *et al.* (2000). In these experiments a vertically falling thin liquid film is heated from the wall side by a heating device. The transverse dimension of the heater is much longer than its width in the streamwise direction. The heater generates a temperature distribution at the film surface which in turn sets up surface tension gradients that drive the fluid away from the heated region. This thermocapillary flow results in the formation of a (two-dimensional) bump in the streamwise direction, the height of which increases as the heat flux supplied by the heater to the liquid increases. At a certain critical value of the heat flux, an instability in the transverse direction develops. This instability, which has a very well-defined wavelength, takes the form of rivulets at the downstream edge of the bump.

In this paper we develop a stability theory for the falling film heated from below. Our analysis is based on the integral-boundary-layer approximation of the Navier–Stokes/energy equations and free-surface boundary conditions. This approximation results in a system of two coupled nonlinear partial differential equations for the evolution of the local height and temperature of the free surface in time and space. Steady states of these equations are reported for different values of the governing dimensionless groups. Our computations reveal that in all cases the free-surface profile develops a ridge upstream of the heater's centre where the wall temperature gradient is positive and a depression downstream of the heater's centre where the wall temperature gradient is negative. We analyse the linear stability of these two-dimensional steady states with respect to disturbances in the spanwise direction. It is shown that the operator of the linearized system has both a continuous and a discrete spectrum. The discrete spectrum arises from resonance poles at certain wavenumbers for the disturbances in the spanwise direction. The continuous spectrum is always stable, while part of the discrete spectrum is destabilized for values of the Marangoni number (which expresses the relative importance of thermocapillary and viscous stresses) larger than a critical value. Above this critical Marangoni number the growth rate curve as a function of wavenumber has a finite band of unstable modes which becomes larger as the Marangoni number increases.

2. Formulation

We consider a thin liquid film of viscosity μ, surface tension σ and density ρ falling down an inclined planar wall with inclination angle θ with respect to the horizontal direction. Figure 1 sketches the flow situation. The wall is heated by a local heat source, $T = f(x)$, $f(x) \to 0$ as $x \pm \infty$, with T the temperature of the wall. This temperature distribution can be produced, for example, by a heating device. This heater, perpendicular to the plane of figure 1, supplies heat under the film flowing over the substrate and generates a temperature distribution at the film surface which in turn sets up surface tension gradients. These Marangoni stresses will drive the fluid away from the heated region; however, sufficiently far from the heat source, the

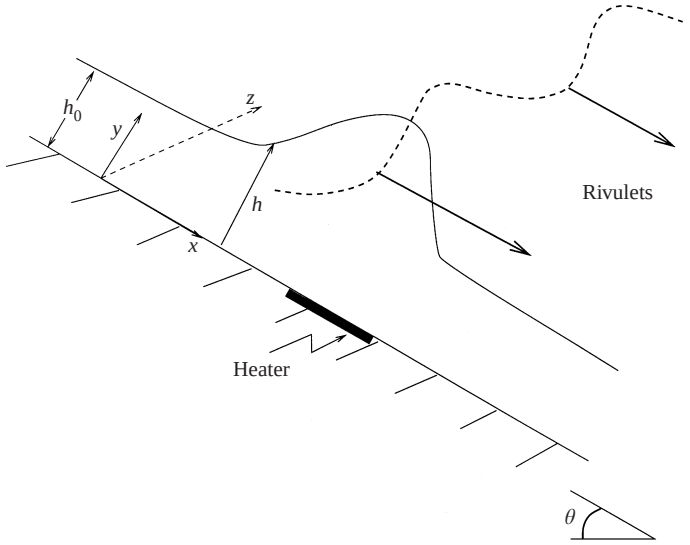

FIGURE 1. Sketch of the profile geometry for flow down a heated inclined plane. The film thickness is $h(x, z, t)$; h_0 is the film thickness far from the heater.

falling liquid film is undisturbed with thickness h_0 and velocity distribution

$$U = \frac{g}{v} \sin\theta (h_0 y - \tfrac{1}{2} y^2), \tag{1}$$

which gives the Nusselt velocity $u_0 = g h_0^2 \sin\theta / 3v$ where g the gravitational acceleration and $v = \mu/\rho$ the kinematic viscosity of the liquid.

Because of the extreme complexity of the full Navier–Stokes equation with nonlinear free-surface boundary conditions, most nonlinear studies on thin film flows (with and without Marangoni effects) have been based on the long-wave lubrication approximation (see for instance the review by Oron *et al.* 1997). With this approximation, the Navier–Stokes equation reduces to a single, highly nonlinear, partial differential equation commonly known as the evolution equation for the location of the interface. In this study we adopt the integral-boundary-layer approximation (IBL), first introduced by Shkadov (1967). Unlike the usual long-wave lubrication approximation, subsequently referred to as Benney's approximation (see Benney 1966), where relative orders of the film amplitude and the governing dimensionless groups, namely Reynolds number and Weber number, are assigned *a priori*, the IBL equation is derived with only the long-wave expansion and without overly restrictive stipulations on the order of the amplitude and the dimensionless groups. The original IBL approximation though was restricted to free-surface thin film flows in the absence of thermal effects. Here, we extend the approximation to include heat transport and we derive an averaged energy equation for the temperature distribution on the free surface.

The starting point of the IBL approach is to assume long waves in both the x- and z-directions, i.e. $\partial/\partial x$, $\partial/\partial z \ll \partial/\partial y$ and $v, w \ll u$ with u, v and w the x, y and z components of velocity respectively. With this assumption and after scaling x, y and z with h_0, velocities u, v, w with u_0, time with h_0/u_0 (the time an interfacial particle transverses a distance h_0), pressure P with ρu_0^2 and temperature T with ΔT (the difference between the maximum temperature of the heat source and the temperature

of the liquid far from the source), the equations of motion and energy equation are simplified to

$$\frac{\partial u}{\partial t}+\frac{\partial u^2}{\partial x}+\frac{\partial uv}{\partial y}+\frac{\partial uw}{\partial z}+\frac{3\cot\theta}{Re}\frac{\partial h}{\partial x}=We\frac{\partial K}{\partial x}+\frac{1}{Re}\left(\frac{\partial^2 u}{\partial y^2}+3\right), \tag{2a}$$

$$\frac{\partial w}{\partial t}+\frac{\partial wu}{\partial x}+\frac{\partial wv}{\partial y}+\frac{\partial w^2}{\partial z}+\frac{3\cot\theta}{Re}\frac{\partial h}{\partial z}=We\frac{\partial K}{\partial z}+\frac{1}{Re}\frac{\partial^2 w}{\partial y^2}, \tag{2b}$$

$$\frac{\partial T}{\partial t}+\frac{\partial}{\partial x}(Tu)+\frac{\partial}{\partial y}(Tv)+\frac{\partial}{\partial z}(Tw)=\frac{1}{Pe}\frac{\partial^2 T}{\partial y^2}, \tag{2c}$$

where K denotes the curvature of the free surface in the long-wave approximation, i.e. $K=-(h_{xx}+h_{zz})$. The Reynolds, Weber and Péclet numbers are defined as

$$Re=\frac{1}{3}\frac{gh_0^3}{\nu^2}\sin\theta, \tag{3a}$$

$$We=\frac{\sigma_0}{\rho h_0 u_0^2}=\frac{3^2\sigma_0\nu^2}{\rho g^2 h_0^5(\sin\theta)^2}=\frac{3^{1/3}\gamma}{Re^{5/3}(\sin\theta)^{1/3}}, \tag{3b}$$

$$Pe=Re\,Pr=Re\frac{a}{\nu}, \tag{3c}$$

where σ_0 the surface tension at a reference temperature T_0 and a the thermal diffusivity ($=k/\rho c_P$ with c_P the constant-pressure heat capacity and k the thermal conductivity of the liquid phase). The Weber number in (3b) expresses the relative importance of surface tension and inertia forces, unlike the usual definition of the Weber number as $\sigma_0/(\rho g\sin\theta h_0^2)$, i.e. the ratio of surface tension over gravity, used frequently in studies of free-surface thin film flows (see for instance Nakaya 1975). Notice, however, that $Re\,We=3\sigma_0/(\rho g\sin\theta h_0^2)$. Also, $\gamma=\sigma_0\rho^{-1}\nu^{-4/3}g^{-1/3}$ is the Kapitza number, a popular parameter among the Russian school, which is only a function of the fluid properties and not the flow conditions, Pr is the Prandtl number and Pe the Péclet number that expresses the relative importance of convection and conduction.

In the derivation of (2) from the full Navier–Stokes equation, we have neglected the second derivatives $\partial^2/\partial x^2$, $\partial^2/\partial z^2$ of the velocity components compared to $\partial^2/\partial y^2$ but we have kept the inertia terms (appropriately modified by using the continuity equation $u_x+v_y+w_z=0$) and the pressure gradients P_x and P_z – see the study by Demekhin & Shkadov (1984) for a detailed derivation of (2). The pressure is obtained from the long-wave expansion of the y-component of the equation of motion, $P_y=-3\cot\theta/Re$, and the long-wave expansion of the normal stress balance, $P=-We\,K$ at $y=h(x,z,t)$, the location of the free surface. The result is $P=3\cot\theta(h-y)/Re-We\,K$. The analogy with the classical boundary-layer theory is now clear: in the boundary-layer, inertia balances viscous diffusion in the y-direction and the pressure gradient in the x-direction and it is this balance that gives rise to the Blasius profile. However, unlike boundary-layer theory where the pressure gradient is imposed by the inviscid flow and is related to velocity via Bernoulli's equation, in our case the pressure gradient is self-induced and caused by the capillary forces at the interface.

Using a linear approximation for the surface tension,

$$\sigma=\sigma_0-\kappa(T-T_0), \tag{4}$$

with $\kappa>0$ for typical liquids, the boundary conditions for the velocities u and w at

the free surface are

$$\frac{\partial u}{\partial y} = -Ma\frac{\partial T}{\partial x}, \quad y = h(x,z,t), \tag{5a}$$

$$\frac{\partial w}{\partial y} = -Ma\frac{\partial T}{\partial z}, \quad y = h(x,z,t), \tag{5b}$$

the long-wave expansions of the tagential stress balance at the free surface. Ma is the Marangoni number defined as

$$Ma = \frac{\kappa\Delta T}{\mu u_0} = \frac{3\kappa\Delta T}{\rho g h_0^2(\sin\theta)^2} \tag{6}$$

and expresses the relative importance of thermocapillary and viscous stresses. The boundary condition for T at the interface is Newton's law of cooling in which the heat flux normal to the interface is analogous to the temperature difference between the interface and the ambient gas phase. The long-wave approximation of this condition yields

$$\frac{\partial T}{\partial y} + Bi(T - T_a) = 0, \tag{7}$$

where $Bi = \alpha h_0/k$, the Biot number, with α the heat transfer coefficient describing the rate of heat transport from the liquid to the ambient gas phase at the constant temperature T_a. We also have the kinematic boundary condition at the interface

$$\frac{\partial h}{\partial t} + \frac{\partial}{\partial x}\int_0^h u\,\mathrm{d}y + \frac{\partial}{\partial z}\int_0^h w\,\mathrm{d}y = 0, \quad y = h(x,z,t), \tag{8}$$

and the no-slip boundary condition on the wall

$$u = v = w = 0, \quad y = 0. \tag{9}$$

Finally,

$$T = f(x), \quad y = 0, \tag{10}$$

with $f(x)$ the temperature distribution generated by the heater on the wall.

An *ad hoc* and convenient simplification of the above equations and boundary conditions can be made by assuming a self-similar parabolic profile beneath the film (Schkadov 1967; Demekhin & Schkadov 1984). In the presence of Marangoni stresses this profile is taken to be

$$u = \frac{3q}{h}(\eta - \tfrac{1}{2}\eta^2) + \tfrac{1}{2}Ma\frac{\partial T_s}{\partial x}h(\eta - \tfrac{3}{2}\eta^2), \tag{11a}$$

$$w = \frac{3p}{h}(\eta - \tfrac{1}{2}\eta^2) + \tfrac{1}{2}Ma\frac{\partial T_s}{\partial z}h(\eta - \tfrac{3}{2}\eta^2), \tag{11b}$$

where

$$\eta = \frac{y}{h(x,z,t)} \tag{11c}$$

$$q = \int_0^h u\,\mathrm{d}y, \quad p = \int_0^h w\,\mathrm{d}y, \tag{11d}$$

with T_s the temperature of the interface and q, p the flow rates in the x- and z-directions respectively. These velocity profiles satisfy the boundary conditions (5a, b) and (9). In addition, the integrals of these profiles with respect to y (or the similarity variable η) give the flow rates q and p, as they should (notice that $\eta = y/h(x,z,t)$

is a natural similarity variable to use as the boundary conditions in terms of η are applied at $\eta = 0$ and $\eta = 1$). Hence, the basic assumption here is that a parabolic velocity profile, which satisfies the x-component of the equation of motion for zero Reynolds number, persists even for large Reynolds numbers when the free surface is no longer flat. This assumption has been verified experimentally for falling liquid films (Alekseenko, Nakoryakov & Pokusaev 1994) in the regime of large Reynolds numbers, $Re < 500$. It is well known that wave evolution in a falling film for large Reynolds numbers is characterized by a train of soliton-like coherent structures with almost the same amplitude and which interact indefinitely with each other (see Chang 1994 for a review). Measurements of the velocity profile in these solitary waves indicate that the profile is parabolic throughout except perhaps in a small neighbourhood of a 'dimple' that develops in front of the solitary humps where a deviation from the parabolic profile was observed (this dimple is the first in a series of bow waves that connect the steep front edge of a solitary wave to the flat film ahead).

Obviously, there are several other functional forms which satisfy the boundary conditions at $\eta = 0$ and $\eta = 1$ instead of the ones chosen in (11a, b) (provided that these functions do not induce a reverse flow in the absence of thermocapillary effects). For example, in the absence of Marangoni stresses, $\eta^2 - (2/3)\eta^3$ is one such function. One could then use a Galerkin-type approach to project the velocities onto the (polynomial) test functions which satisfy the boundary conditions. For the IBL approximation we choose the simplest test function, which in the absence of Marangoni stresses is $\eta - (1/2)\eta^2$. Linear stability calculations using this test function also give good agreement with the linear stability from the full Navier–Stokes equation (Ruyer-Quil 2001, personal communication – see also discussion on the validity of this approximation by Ruyer-Quil & Mannevile 1998, 2000, 2002). At the same time, by analogy with laminar boundary-layer theory, we anticipate that the error introduced by the parabolic profile assumption is small – for example Pohlhausen's assumption of a fourth-order polynomial for the velocity profile in the boundary layer gives less than 10% error for the thickness of the boundary layer compared to the Blasius solution.

For the temperature distribution we assume

$$T = f(x) + [T_s(x, z, t) - f(x)]\eta, \tag{12}$$

such that $T = f(x)$ at $\eta = 0$ and $T = T_s$ at $\eta = 1$. The assumption here is that the linear temperature profile obtained for a flat film (and neglecting convective effects in the heat transport process) persists even when the interface is no longer flat. Clearly, this linear temperature profile does not satisfy the free-surface boundary condition (7), unlike the test functions for the velocities in (11a, b), which satisfy all boundary conditions, i.e. (5a, b) and (9). Hence, in weighted residual methods terminology, the approximation (12) is a 'mixed Galerkin method' as the trial solution does not satisfy either the equation or (all) the boundary conditions (the approximation for the velocities is an 'interior' method as the trial functions satisfy the boundary conditions but not the equations – see Ames 1977 for a classification). We now integrate the momentum equation (2a, b) from $y = 0$ to $y = h$, multiply the energy equation (2c) by y and integrate the resulting equation from $y = 0$ to $y = h$ (this process is analogous to the Kármán–Pohlhausen integral method in boundary-layer theory). Several terms in these integral versions of the momentum and energy equations can be simplified by performing integrations by parts. The terms originating from the integrations by parts can be evaluated by using the boundary conditions (5a, b), (7), (9) and (10). Notice that we have implicitly assumed $\epsilon^2 \ll \epsilon Ma \ll 1$, with $\epsilon \ll 1$

the film parameter, the ratio of the average film thickness over a long scale in the streamwise direction. Hence, the Marangoni terms in (11a,b) are of $O(\epsilon Ma)$ (due to the long-wave approximation, $\partial T_s/\partial x$, $\partial T_s/\partial z = O(\epsilon)$) so that they contribute only to the viscous terms $\partial^2/\partial y^2$ of (2a–c) and are neglected in the inertial/convective terms of (2a–c) which are of $O(\epsilon Re)$. Similar arguments can be used to show that $\epsilon^2 \ll \epsilon Re \ll 1$, so that our IBL model contains terms of $O(1)$, $O(\epsilon Ma)$, $O(\epsilon Re)$ and $O(\epsilon)$. Finally, we utilize (11a,b,d) and (12) and after lengthy algebraic manipulations, we obtain the averaged momentum and energy equations:

$$\frac{\partial q}{\partial t} + \frac{6}{5}\frac{\partial}{\partial x}\frac{q^2}{h} + \frac{6}{5}\frac{\partial}{\partial z}\frac{qp}{h} + \frac{3\cot\theta h}{Re}\frac{\partial h}{\partial x} = We\, h\frac{\partial K}{\partial x} + \frac{3}{Re}\left(h - \frac{q}{h^2}\right) - \frac{3Ma}{2Re}\frac{\partial T_s}{\partial x}, \tag{13a}$$

$$\frac{\partial p}{\partial t} + \frac{6}{5}\frac{\partial}{\partial x}\frac{qp}{h} + \frac{6}{5}\frac{\partial}{\partial z}\frac{p^2}{h} + \frac{3\cot\theta h}{Re}\frac{\partial h}{\partial z} = We\, h\frac{\partial K}{\partial z} - \frac{3}{Re}\frac{p}{h^2} - \frac{3Ma}{2Re}\frac{\partial T_s}{\partial z}, \tag{13b}$$

$$\frac{\partial h}{\partial t} + \frac{\partial q}{\partial x} + \frac{\partial p}{\partial z} = 0, \tag{13c}$$

$$\frac{\partial T_s}{\partial t} - \frac{7}{40}\frac{\partial q}{\partial x}\frac{f}{h} - \frac{7}{40}\frac{\partial p}{\partial z}\frac{f}{h} + \frac{7}{40}\frac{\partial q}{\partial x}\frac{T_s}{h} + \frac{7}{40}\frac{\partial p}{\partial z}\frac{T_s}{h} + \frac{21}{40}\frac{\partial f}{\partial x}\frac{q}{h} + \frac{27}{20}\frac{\partial T_s}{\partial x}\frac{q}{h} + \frac{27}{20}\frac{\partial T_s}{\partial z}\frac{p}{h} = \frac{3}{Pe}\left[-\frac{Bi(T_s - T_a)}{h} - \frac{T_s - f}{h^2}\right]. \tag{13d}$$

We note that although (12) does not satisfy the free-surface boundary condition (7), the averaged energy equation (13d) does. Indeed, after we multiply (2c) with the 'weight' function, y, we perform integrations by parts and evaluate the boundary terms which involve T_y from (7) and not (12) (which of course does not satisfy (7)). We hence apply all boundary conditions prior to substituting the linear approximation in (12). For example, multiply the diffusion term T_{yy} in (2c) by y and integrate from $y = 0$ to $y = h$. The result is

$$\int_0^h y T_{yy}\,\mathrm{d}y = hT_y|_{y=h} - (T|_{y=h} - T|_{y=0}) = -hBi(T_s - T_a) - T_s + f.$$

Notice that the weight function for the energy equation is chosen so that the terms resulting from integrations by parts involve either T at $y = 0$ or T_y at $y = h$, i.e. the boundary conditions (7) and (10). Notice also that with this weight function points near the interface ($y = h$) have a 'larger weight' than points near the solid boundary.

Obviously, to balance the curvature gradient with h_x in (2a), $Re\,We$ must be a large number, strictly speaking $We\,Re = O(\epsilon^{-2})$ with respect to the long-wave parameter ϵ that measures the gradient $\partial/\partial x$. Hence, although the term $We\,Re\,K_x$ is formally of third order and thus should not appear at this stage, $We\,Re$ is large enough so that it enters the problem at the same level as $\partial h/\partial x$. This observation originates from the expression for the pressure: $P = 3\cot\theta(h - y)/Re - We\,K$. Hence, we take into account the curvature term at a stage of the long-wave expansion earlier than its formal order, in fact at the lowest possible order, i.e. by assuming that the capillary forces contribute to the evaluation of the pressure at order zero. However, as we have already pointed out, there is no stipulation on the relative order of Re and We.

The case $Re\,We \gg 1$ studied here is commonly referred to as 'the strong surface tension case'. It applies to water and most other liquids but not to fluids with low surface tension, like glycerin. The danger in *a priori* assigning relative orders of Re, We and film amplitude with respect to the long-wave parameter ϵ, as in Benney's

approximation, was recognized by Benney himself. He found that his weakly nonlinear expansions yield either the Burgers equation, the KdV equation, or others depending on the specific assignments made. Since Re and We are independent parameters that specify the wave height and wavelength in terms of the long-wave parameter, these *a priori* assignments often yield equations that cannot describe the full range of waves in falling films. As a result, shock formation for the Burgers equation and unrealistic large-amplitude solutions in certain regimes of the parameter space (Rosenau, Oron & Hyman 1992), including finite-time blow-up behaviour for sufficiently large sets of smooth initial data, occur when these equations are integrated in time and as the waves attempt to evolve into ones beyond their description. In addition, the physical relevance of Benney's equation has been shown to be confined to quite thin films (Oron & Gottlieb 2002). At the same time the IBL approximation has been successful in describing solitary wave dynamics on a falling film and without any unrealistic blow-up behaviour (see for instance Chang, Demekhin & Kopelevich 1993 and Chang 1994). Quantitative agreement between the solitary waves obtained from the IBL equation and experimental wave tracings has also been established by the same authors for $Re < 500$. Hence, in the presence of inertia the IBL approximation for the momentum equations can be considered as the model equation of choice (short of the complete Navier–Stokes equation of course).

For small Reynolds numbers, the inertia terms in (13a, b) can be neglected and the flow rates q, p are adiabatically slaved to the film thickness $h(x, z, t)$ and they depend on time only through the dependence of $h(x, z, t)$ on time:

$$q = h^3 + \frac{We\,Re}{3} h^3 \frac{\partial K}{\partial x} - \cot\theta h^3 \frac{\partial h}{\partial x} - \tfrac{1}{2} Ma\, h^2 \frac{\partial T_s}{\partial x}, \tag{14a}$$

$$p = \frac{We\,Re}{3} h^3 \frac{\partial K}{\partial z} - \cot\theta h^3 \frac{\partial h}{\partial z} - \tfrac{1}{2} Ma\, h^2 \frac{\partial T_s}{\partial z}. \tag{14b}$$

Substituting these expressions into the kinematic boundary condition (13c) gives an evolution equation for the variation of h:

$$\frac{\partial h}{\partial t} + \frac{\partial}{\partial x}\left(h^3 + \frac{We\,Re}{3} h^3 \frac{\partial K}{\partial x} - \cot\theta h^3 \frac{\partial h}{\partial x} - \tfrac{1}{2} Ma\, h^2 \frac{\partial T_s}{\partial x} \right) + \frac{\partial}{\partial z}\left(\frac{We\,Re}{3} h^3 \frac{\partial K}{\partial z} - \cot\theta h^3 \frac{\partial h}{\partial z} - \tfrac{1}{2} Ma\, h^2 \frac{\partial T_s}{\partial z} \right) = 0. \tag{15}$$

Therefore, the equation for the film thickness in the limit of vanishing inertia becomes identical to the usual lubrication approximation without inertia. Hence, the usual long-wave expansion for $Re = 0$ is a *limiting case* of the IBL approximation. This limit of vanishing inertia is consistent with the experiments reported by Kabov *et al.* (1996, 1999), Kabov (1998) and Scheid *et al.* (2000) which indicate that the instability develops for a large region of Reynolds numbers including small Reynolds numbers and those as large as $O(1)$ or larger.

Equations (15) and (13d) with the flow rates given by (14a, b) are the basic equations for the analysis to follow. Hence, unlike the flow rates, the temperature distribution on the free surface is not slaved to the film thickness and although the film thickness is described by the usual long-wave approximation (effectively Benney's equation without inertia) the temperature distribution on the free surface is described by the IBL approximation of the energy equation. The assumption that the temperature field is adiabatically slaved to the film thickness has often been used in the literature (Joo *et al.* 1991; Burelbach *et al.* 1988; Bankoff 1994; Oron 1999; Oron & Peles

1998). From (13*d*) this is effectively the case when $Pe \ll 1$. In this limit, convection is negligible compared to heat diffusion and the interface temperature is simply given by

$$T_s = \frac{f + Bi\, T_a h}{1 + Bi\, h}. \tag{16}$$

Substitution of this temperature distribution in (15) gives the evolution equation for the film thickness used for example by Joo *et al.* (1991). The same temperature distribution was also adopted recently by Scheid *et al.* (2001). These authors used Benney's equation with inertia to describe the one-dimensional evolution of the interface for the thermocapillary problem considered here. They performed time-dependent computations of Benney's equation for the one-dimensional evolution of the free surface and for a uniform wall temperature distribution or a sinusoidal function of x. They reported a variety of solutions including oscillatory modes, travelling waves and standing waves.

Obviously, if the interface is a poor conductor and perfectly insulated from the gas, $Bi \ll 1$, and (16) shows that $T_s = f(x)$. This assumption was utilized by Gramlich *et al.* (2002) in their study of optimal levelling of free-surface thin film flows over topography by means of a thermocapillary stress induced by a localized heater on the topographical substrate. However, for the thermocapillary instability problem considered here, the experiments by Kabov *et al.* (1996, 1999), Kabov (1998) and Scheid *et al.* (2000) clearly indicate that the temperature distributions on the free surface are very different from (16). In fact, the Péclet number in these experiments is $O(1)$ or even larger and clearly convection at finite Péclet number will lead to a convective distortion of the surface temperature profile (16), which assumes negligible convection. Therefore, the temperature field is convected downstream and hence we utilize the full convection/diffusion equation (13*d*) coupled to the evolution equation for the film thickness (15).

3. Steady states

Let us now consider two-dimensional stationary solutions of the system (13*d*) and (15) with the flow rates given from (14*a*, *b*). With $h = h(x)$, $q = 1$, $p = 0$ and $T_s = T_s(x)$, we obtain a system of two coupled ordinary differential equations for $h(x)$ and $T_s(x)$:

$$Re\, We\, h \frac{\mathrm{d}^3 h}{\mathrm{d}x^3} - \frac{3\cot\theta}{2Re}\frac{\mathrm{d}h}{\mathrm{d}x} - \frac{3Ma}{2Re}\frac{\mathrm{d}T_s}{\mathrm{d}x} + 3\left(h - \frac{1}{h^2}\right) = 0, \tag{17a}$$

$$\frac{9}{20}\frac{\mathrm{d}T_s}{\mathrm{d}x} + \frac{7}{40}\frac{\mathrm{d}f}{\mathrm{d}x} + \frac{Bi}{Pe}T_s = \frac{1}{Pe}\frac{f - T_s}{h}, \tag{17b}$$

where we assumed $T_a = 0$ without loss of generality. The wall temperature profile is taken to be

$$f(x) = \mathrm{e}^{-bx^2}, \quad b = 0.005, \tag{18}$$

which can be viewed as a model of a wire enclosed by a partially thermally conductive material. (In the thermocapillary levelling study by Gramlich *et al.* 2002 a variety of wall temperature profiles was examined including (18) and a rectangular 'top-hat' temperature distribution as a model of a resistively heated wire perfectly insulated at the upstream and downstream edges.) The boundary conditions for (17) are $h \to 1$ as $x \to \pm\infty$ with all the derivatives of h approaching zero at the infinities and $T_s \to 0$

as $x \to \pm\infty$ (i.e. T_s approaches the ambient temperature) with all the derivatives of T_s approaching zero at the infinities as well.

A point to be noted here is that the wall temperature distribution in (18) introduces a lengthscale in the streamwise direction analogous to $b^{-1/2}$. Hence, unlike the case of a liquid film falling down a uniformly heated plane, where the long scale in the streamwise direction is not known *a priori*, for the problem of a falling film heated from below by a local heat source, this lengthscale can be taken as the characteristic lengthscale of the wall temperature distribution. We could then consider a long-wave expansion with respect to two small parameters: the film parameter ϵ, and the small parameter that measures the ratio of the amplitude of the wall temperature distribution (this is 1 for the function in (18)) and the scale in the streamwise direction, say ϵ_1. Here we have implicitly assumed the distinguished limit $\epsilon \sim \epsilon_1$ or $b \sim \epsilon^2$ in the derivation of our IBL approximation.

We solve (17a, b) numerically with a global Fourier spectral expansion in the streamwise coordinate x:

$$h(x) = \int_{-\infty}^{+\infty} \tilde{H}(\omega)\, \mathrm{e}^{\mathrm{i}\omega x}\, \mathrm{d}\omega \simeq \sum_{-N}^{+N} H_k \mathrm{e}^{\mathrm{i}\delta k x}\delta, \tag{19a}$$

$$T_s(x) = \int_{-\infty}^{+\infty} \tilde{T}(\omega)\, \mathrm{e}^{\mathrm{i}\omega x}\, \mathrm{d}\omega \simeq \sum_{-N}^{+N} T_k \mathrm{e}^{\mathrm{i}\delta k x}\delta, \tag{19b}$$

$$H_k = H_{-k}^*, \quad T_k = T_{-k}^*, \tag{19c}$$

where $\tilde{H}$, $\tilde{T}$ are the Fourier transforms of h, T_s, i.e. we seek the solutions in terms of Fourier integrals which for numerical purposes are approximated by sums, with $\delta = 2\pi/L$ where L is the periodicity interval in the x-direction. $H_k\delta$ and $T_k\delta$ are the discrete approximations of $\tilde{H}$ and $\tilde{T}$. This definition facilitates the numerical implementation of our pseudospectral method as it makes the coefficients H_k and T_k relatively independent of the periodicity interval L. Equation (19c) ensures that the sums in (19a, b) are real quantities (the stars in (19c) denote complex conjugation). We then substitute (19a, b) into (17a, b) and apply the resulting equations at $4N + 2$ points in the interval $[-L/2, L/2]$. Therefore, we obtain a set of $(4N + 2)$ nonlinear algebraic equations for the $(4N + 2)$ unkowns in (19a, b) which we solve using Newton's method. The nonlinear terms in (17a, b) are calculated in physical space and the Newton iteration, which involves inversion of a sparse matrix containing the projected linear terms, is carried out in Fourier space with the aid of a fast Fourier tranform.

The initial guess in Newton's method is obtained from the limit $Ma \to 0$. In this limit, the influence of the temperature field on the free surface is small and as a first approximation we can take $h = 1$ and solve the linear energy equation

$$\frac{\mathrm{d}T_s}{\mathrm{d}x} + \frac{20}{9}\frac{1 + Bi}{Pe}T_s = -\frac{7}{18}\frac{\mathrm{d}f}{\mathrm{d}x} + \frac{20}{9}\frac{1}{Pe}f, \tag{20}$$

which can be easily solved analytically in Fourier space for a given f (that is localized and decays sufficiently fast at infinity). With T_s known from (20), we turn to the free-surface equation (17a) and obtain h by assuming that the deviation from 1 is small, i.e. $h = 1 + \bar{h}$, $\bar{h} \ll 1$:

$$Re\, We\frac{\mathrm{d}^3\bar{h}}{\mathrm{d}x^3} - (3\cot\theta + 9)\frac{\mathrm{d}\bar{h}}{\mathrm{d}x} = \tfrac{3}{2}Ma\frac{\mathrm{d}T_s}{\mathrm{d}x} \tag{21}$$

for some small value of Ma. This equation can also be solved analytically in Fourier space. Using the solution found for small Ma as initial guess for Newton's method, we utilize a continuation technique to continue the solution to the region of large Marangoni numbers. The accuracy of the numerical scheme was determined by variation of the domain size and number of points in the domain.

We found that convergence of this numerical scheme required a large number of harmonics, mainly due to the mixed parabolic/hyperbolic character of our IBL system (17a, b) and the fact that the resulting temperature profile on the free surface is much more localized than the free surface itself. Hence, from a numerical point of view it is more efficient to avoid solving for $h(x)$ and $T_s(x)$ simultaneously unless we introduce in (17) a second derivative T_{sxx} multiplied by a small parameter, in which case convergence is substantially improved. Alternatively, we implement a domain pertubation scheme in which we solve the convection/diffusion equation (17b) to obtain the temperature distribution on the free surface, assuming the free surface is flat. Using this temperature profile, we solve for the free-surface deflection in (17a) and we subsequently substitute the new free-surface profile into (17b). We repeat this process until convergence for both h and T_s is achieved (we also utilized a continuation technique with respect to Ma).

Figure 2 shows typical free-surface profiles at different Marangoni numbers for $\theta = \pi/2$, $Re = 1$, $Bi = 1$, $\gamma = 2850$ and $Pr = 7$ (these values of γ and Pr are for water at 25°). Obviously, the value $Re = 1$ violates the basic assumption of small inertia for the derivation of (15) and its steady version (17a). The issue of whether or not the inertia terms of the IBL approximation introduce fundamentally new features or just a quantitative correction to the usual long-wave expansion for the free surface in (15) will be treated in a future paper. Alternatively, figure 2 depicts the free surface at different values of Marangoni numbers for $\theta = \pi/2$, $Bi = 1$, $We\,Re = 4110$ and $Pe = 7$. These values of the flow parameters do allow for small Re and at the same time the assumption $We\,Re \gg 1$ for the IBL approximation (2) is satisfied.

As can be seen from figure 2, the free-surface profile has a depression just downstream of the location of the heater, $x = 0$, where the wall temperature gradient is negative and a ridge just upstream of $x = 0$ where the wall temperature gradient is positive. A bump on the free surface has also been observed in the experimental studies by Kabov *et al.* (1996, 1999), Kabov (1998) and Scheid *et al.* (2000). This standing wave appears as a result of the nonlinear interaction between the liquid flowing downstream due to gravity and the reverse thermocapillary flow induced by the heater (in fact Kabov refers to this standing wave as the 'liquid roller'). Notice from figure 2 that the height of the bump increases as the Marangoni number increases. This observation is also consistent with the experiments in which the height of the bump was found to be an increasing function of the heat flux provided by the heater.

The steady states for thin film flows over planar walls heated by local heat sources have also been examined using standard lubrication theory by Gramlich *et al.* (2002), Marchuk & Kabov (1998) and Scheid *et al.* (2001). A variety of wall temperature distributions was examined by Gramlich *et al.* (2002) while Scheid *et al.* (2001) adopted the difference between two inverse tangent functions as a model for the wall temperature shape. All these authors observed bumps on the free surface located roughly at the point where the wall temperature distribution has a maximum. Marchuk & Kabov (1998), in particular, used two different boundary conditions on the solid boundary: a given temperature distribution and a given flux. In some cases the wall temperature distribution was chosen so that the total heat flux from the heater to

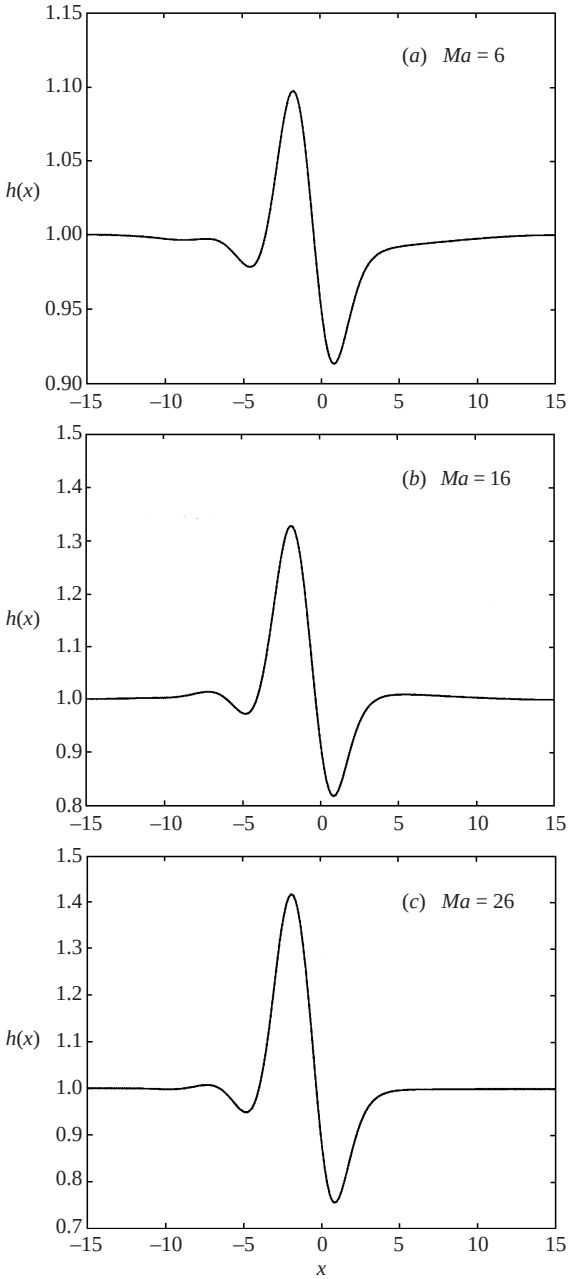

FIGURE 2. Free-surface profiles at different Marangoni numbers for $\theta = \pi/2$, $Re = 1$, $\gamma = 2850$, $Pr = 7$ and $Bi = 1$.

the film was in agreement with the specified heat flux. Interestingly, both boundary conditions gave similar results for the free surface.

Figure 3 depicts the temperature distributions on the free surface for the profiles in figure 2. Unlike the wall temperature, the free-surface temperature is asymmetric, with a maximum downstream of the heater's centre at $x = 0$: due to the finite Péclet number convection the temperature field is convected downstream. Notice that the

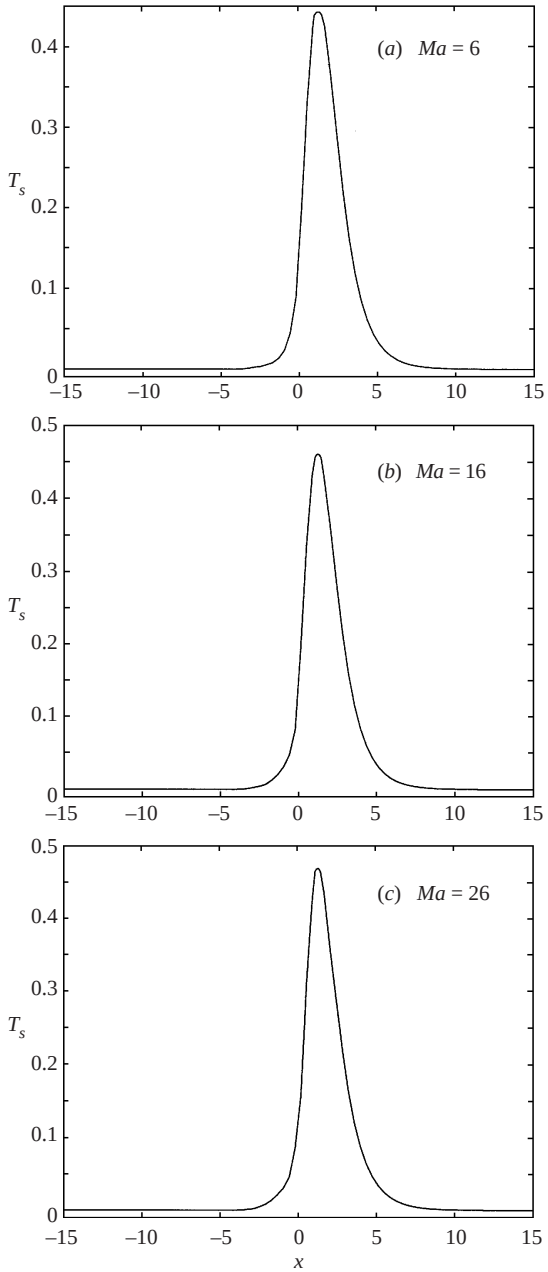

FIGURE 3. Temperature distributions on the free surface for the profiles in figure 2.

temperature maximum increases slowly as the Marangoni number Ma increases (unlike the maximum of the free surface height which increases faster as Ma increases – see figure 2). Finally, when the wall temperature is very localized in space, effectively approaching a Dirac function (this is the case of large b), T_s approaches the derivative of a Dirac function and will take negative values in a small region upstream of the heater's centre. As T_s is always positive (or larger than the temperature of the ambient gas phase – recall that we set $T_a = 0$ in (17) and hence figure 3 shows the surface tem-

perature relative to the ambient temperature) negative temperatures are a consequence of the long-wave approximation which is expected to break down when the gradient of the forcing function f is large. Hence, provided that $b \ll 1$, for the long-wave approximation to be valid, the interface temperature distribution is always positive.

4. Linear stability

We now examine the stability of the steady states computed in the previous section with respect to infinitesimal disturbances in the spanwise direction. Let

$$h \to h(x) + v\hat{h}(x)\,\mathrm{e}^{\lambda t}\mathrm{e}^{\mathrm{i}\beta z} + \text{c.c.}, \tag{22a}$$

$$T_s \to T_s(x) + v\,\hat{T}(x)\,\mathrm{e}^{\lambda t}\mathrm{e}^{\mathrm{i}\beta z} + \text{c.c.}, \tag{22b}$$

with $v \ll 1$. Substituting these normal modes into the system (13d), (14a, b) and (15) and utilizing the steady-state equations (17a, b), yields the infinite-domain eigenvalue problem

$$\mathscr{L}\begin{bmatrix} \hat{h} \\ \hat{T} \end{bmatrix} + \lambda \begin{bmatrix} \hat{h} \\ \hat{T} \end{bmatrix} = 0 \tag{23a}$$

with boundary conditions

$$\hat{h}, \hat{T} \quad \text{bounded} \quad \text{as} \to \pm\infty. \tag{23b}$$

The elements of the matrix/differential operator $\mathscr{L} = [\mathscr{L}_{ij}]$ are defined as

$$\mathscr{L}_{11} = S_1\frac{\mathrm{d}^4}{\mathrm{d}x^4} + S_2\frac{\mathrm{d}^3}{\mathrm{d}x^3} + S_3\frac{\mathrm{d}^2}{\mathrm{d}x^2} + S_4\frac{\mathrm{d}}{\mathrm{d}x} + S_5, \tag{24a}$$

$$\mathscr{L}_{12} = S_6\frac{\mathrm{d}^2}{\mathrm{d}x^2} + S_7\frac{\mathrm{d}}{\mathrm{d}x} + S_8, \tag{24b}$$

$$\mathscr{L}_{21} = G_1\frac{\mathrm{d}^4}{\mathrm{d}x^4} + G_2\frac{\mathrm{d}^3}{\mathrm{d}x^3} + G_3\frac{\mathrm{d}^2}{\mathrm{d}x^2} + G_4\frac{\mathrm{d}}{\mathrm{d}x} + G_5, \tag{24c}$$

$$\mathscr{L}_{22} = G_6\frac{\mathrm{d}^2}{\mathrm{d}x^2} + G_7\frac{\mathrm{d}}{\mathrm{d}x} + G_8, \tag{24d}$$

where the coefficients G_i and S_i are given in the Appendix.

The boundary conditions in (23b) allow for eigenfunctions which do not decay to zero but approach bounded oscillations at the infinities. We shall demonstrate that there are two types of singularities associated with the spectrum of $\mathscr{L}$: discrete eigenvalues and the continuous essential spectrum. The discrete spectrum consists of decaying eigenfunctions with $\hat{h}(\pm\infty) = \hat{T}(\pm\infty) = 0$. These eigenfunctions correspond to disturbances localized around the base state. The continuous spectrum consists of those eigenfunctions with bounded oscillatory behaviour as $x \to \pm\infty$ and unlike the discrete modes, the essential modes can alter the base flow/temperature distribution far from the ridge/depression configuration of figure 2 and can be associated with disturbances on the thin film regions away from the heater. Such disturbances, sufficiently far from the heater, must be expressed in terms of the continuous modes which do not decay to zero but approach bounded oscillations at the infinities – but still within the bounds where the infinite-domain formulation is valid. This is analogous to expansion of finite-mass disturbances with Fourier modes. Such disturbances correspond to step changes in the average interfacial height/temperature which generate effective point sources or sinks of liquid or heat. At the same time,

as the continuous eigenfunctions do not decay to zero at the infinities, they represent spatially global modes reflecting the response of the base state away from the heater.

The rivulet instability observed in the experiments by Kabov *et al.* (1996, 1999), Kabov (1998) and Scheid *et al.* (2000) is reminiscent of another free-surface thin film problem where a ridge is also present: the problem of a contact line driven by a body force (Troian *et al.* 1989; Bertozzi & Brenner 1997; Spaid & Homsy 1996). In the moving contact line problem, the formation of the ridge is due to the response of the free surface to pressure build-up in the vicinity of the contact line as a result of the kinematic requirement that the streamwise velocity gradually decays as the contact point is approached and then reverses as fluid leaves the contact line region (Goodwin & Homsy 1991). This capillary ridge is known to become unstable to spanwise perturbations and such instabilities have been analysed by a number of authors (Troian *et al.* 1989; Bertozzi & Brenner 1997; Spaid & Homsy 1996; Kondic & Bertozzi 1999; Ye & Chang 1999; Kalliadasis 2000). We note that for the driven contact line problem on a planar inclined substrate, the pertinent eigenvalue problem for $\beta = 0$ has a one-dimensional null space spanned by the eigenfunction associated with the translational invariance of the system in the streamwise direction (Troian *et al.* 1989). This translational invariance manifests itself as a null eigenfunction at $\beta = 0$ corresponding to the eigenvalue $\lambda = 0$ (Kalliadasis 2000) and as the system possesses no other symmetry except the translational invariance, the zero eigenvalue is generically simple. In our case, however, the presence of the heater, which provides a temperature distribution $f(x)$ on the wall, breaks the translational symmetry and hence $\lambda = 0$ is not an eigenvalue for disturbances of infinite wavelength that decay to zero at infinity.

Hence, the situation here is similar to the stability of free-surface thin film flows over topography recently examined by Kalliadasis & Homsy (2001). In this case, the capillary pressure induced by the topography creates interfacial curvature and therefore a capillary pressure that influences the flow features, and for a step-down in topography causes the formation of a capillary ridge just before the entry to the step. Kalliadasis & Homsy analysed the stability of this capillary ridge with respect to infinitesimal disturbances in the spanwise direction and demonstrated that it is stable for all values of the pertinent dimensionless groups. However, for the thermocapillary problem considered here, we shall demonstrate that there exists a critical Marangoni number above which the base flow of figure 2 becomes linearly unstable with respect to disturbances in the spanwise direction.

The behaviour of the eigenfunction $[\hat{h}, \hat{T}]^t$ as $x \to \pm\infty$ can be determined by setting $h = 1$ and $T_s = 0$ in (23*a*). In this case $\mathscr{L}$ becomes a matrix/differential operator with constant coefficients and the eigenvalue problem takes the form

$$\lambda\hat{h} + 3\hat{h}' + \frac{Re\,We}{3}(\hat{h}^{\mathrm{iv}} - 2\beta^2\hat{h}'' + \beta^4\hat{h}) = 0 \tag{25a}$$

$$\lambda\hat{T} + \frac{27}{20}\hat{T}' + \frac{3(1+Bi)}{Pr\,Re}\hat{T} = 0. \tag{25b}$$

Substituting $\hat{h} \sim \mathrm{e}^{\sigma x}$ in (25*a*) gives a fourth-order characteristic polynomial for σ parameterized by λ and β. Hence, there are four 'spatial' eigenvalues for a given $\lambda = \lambda_R + \mathrm{i}\lambda_I$ in the (λ_R, λ_I) spectral plane. For some specific values of λ, σ is purely imaginary and equal to $\mathrm{i}\alpha$. This is the locus Γ_1 of the essential spectrum and is defined by

$$\Gamma_1 = \left\{\alpha\colon \frac{Re\,We}{3}(\alpha^2+\beta^2)^2 + 3\mathrm{i}\alpha + \lambda = 0, \alpha \in (-\infty, +\infty)\right\}. \tag{26a}$$

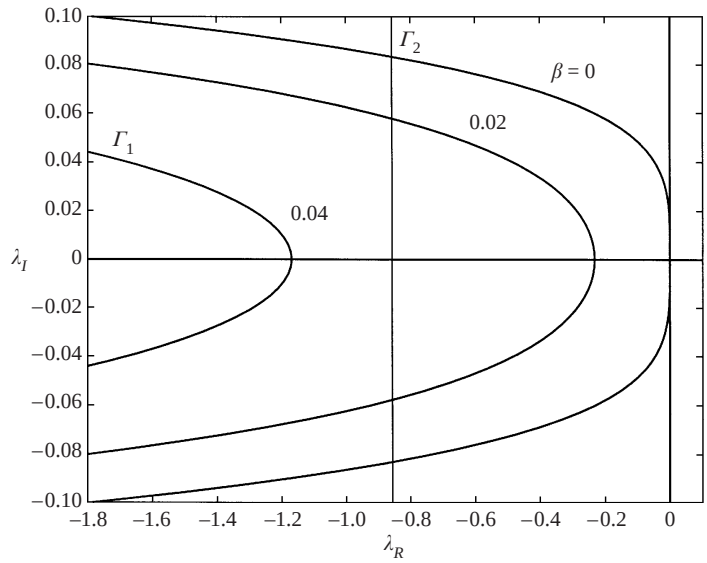

FIGURE 4. Loci of the essential spectrum Γ_1 and Γ_2 in the spectral plane (λ_R, λ_I) at different wavenumbers β for $\theta = \pi/2$, $Re = 1$, $\gamma = 2850$, $Pr = 7$ and $Bi = 1$.

The essential eigenfunctions $\psi(x, \alpha)$ on Γ_1 approach bounded oscillations with wavenumber α at the infinities, i.e. $\psi(x, \alpha) \to e^{i\alpha x}$ as $x \to \pm\infty$.

Consider now (25*b*). Notice that $G_6 \to 0$ as $x \to \pm\infty$ since both T_s and f approach zero at the infinities (see the definition of G_6 in the Appendix). Therefore $\hat{T}$ satisfies a first-order ordinary differential equation as $x \to \pm\infty$. The only bounded (non-trivial) solution to this equation is $\hat{T} = \text{const.}$ for λ in the locus Γ_2 of the continuous spectrum defined from

$$\Gamma_2 = \left\{ \alpha : \frac{3(1 + Bi)}{Pe} + \frac{27}{20} i\alpha + \lambda = 0, \alpha \in (-\infty, +\infty) \right\}. \tag{26b}$$

Hence, there are two branches for the essential spectrum in the complex-λ spectral plane. We note that there is no coupling between $\hat{h}$ and $\hat{T}$ as $x \to \pm\infty$; obviously this is not the case in the neighbourhood of the heater. Figure 4 depicts both branches Γ_1 and Γ_2 for $\theta = \pi/2$, $Re = 1$, $\gamma = 2850$, $Pr = 7$, $Bi = 1$ and different β. Decreasing β shifts the Γ_1 branch to the left and eventually Γ_1 passes through the origin for $\beta = 0$. The second branch Γ_2 is simply a straight line parallel to the λ_I-axis and independent of β. Clearly both branches of the essential spectrum are stable with $\lambda_R \leqslant 0$. Hence, whether the disturbances $\hat{h}$ and $\hat{T}$ grow in time is solely determined by the discrete part of the spectrum.

However, the disturbances must be written as a superposition of both the continuous and discrete modes:

$$\hat{h}(x, t) = \int_{-\infty}^{+\infty} A(\alpha) \psi(x, \alpha) e^{\lambda(\alpha) t} \, d\alpha + \sum_{1}^{N} A_k \psi_k(x) e^{\lambda_k t} \tag{27}$$

as the complete set of functions is formed by combining the eigenfunctions of both spectra – a similar expansion can also be written for the temperature field. Here $\psi(x, \alpha)$ are the essential eigenfunctions and $\psi_k(x)$ the discrete modes. The coefficients $A(\alpha)$ and A_k of the eigenfunction expansion in (27) depend on the initial

condition for the initial value problem for the disturbances $\partial[h, T_s]^t/\partial t + \mathscr{L}[h, T_s]^t = 0$, with $h = h_0(x), T_s = T_{s0}(x)$ at $t = 0$, $\lim_{x\to\pm\infty} h_0(x) = 0$, $\lim_{x\to\pm\infty} T_{s0}(x) = 0$, and can be evaluated by taking the appropriate inner products with the adjoint discrete and continuous eigenfunctions; the adjoint operator $\mathscr{L}^*$ of $\mathscr{L}$ can be found from $\langle \mathscr{L}\boldsymbol{F}, \boldsymbol{G}\rangle = \langle \boldsymbol{F}, \mathscr{L}^*\boldsymbol{G}\rangle$ with respect to the usual $L^2(-\infty, +\infty)$ inner product $\langle \boldsymbol{F}, \boldsymbol{G}\rangle = \int_{-\infty}^{+\infty} \boldsymbol{F}^t \cdot \boldsymbol{G}\,\mathrm{d}x$ for any two vector functions $\boldsymbol{F}$, $\boldsymbol{G}$ in $(-\infty, +\infty)$. However, the exact values of the coefficients in (27) are not important as long as the initial condition is sufficiently rich that the pertinent $A(\alpha)$ and A_k are not zero.

We numerically construct both the discrete and essential spectra with a global Fourier spectral expansion for the eigenfunction $[\hat{h}, \hat{T}]^t$:

$$\hat{h}(x) = \sum_{-N}^{+N} \hat{h}_k \, \mathrm{e}^{\mathrm{i}\delta k x}\delta, \tag{28a}$$

$$\hat{T}(x) = \sum_{-N}^{+N} \hat{T}_k \, \mathrm{e}^{\mathrm{i}\delta k x}\delta, \tag{28b}$$

where $\delta = 2\pi/L$ with L the periodicity interval in the streamwise direction. The infinite interval corresponds to the limit $\delta \to 0$. Substituting (28*a*, *b*) into (23*a*) and isolating the terms associated with the same harmonics yields a homogeneous system of linear algebraic equations for the $(4N + 2)$ complex unkowns $\hat{h}_k$ and $\hat{T}_k$. For the system to have non-trivial solutions it is necessary and sufficient that its principal determinant be equal to zero. Thus, we have converted the differential eigenvalue problem into an algebraic eigenvalue problem of the form

$$\det ||\boldsymbol{A} - \lambda \boldsymbol{I}|| = 0, \tag{29}$$

where $\boldsymbol{A}$ is a $(4N + 2) \times (4N + 2)$ matrix and $\boldsymbol{I}$ is the unitary matrix. Therefore, both essential and discrete eigenvalues of $\mathscr{L}$ are now represented by the eigenvalues of the matrix $\boldsymbol{A}$. To obtain the elements of $\boldsymbol{A}$ from (23*a*) we used forward and backward Fourier transforms for the coefficients S_i, G_i in (24). The eigenvalues were obtained by reducing the matrix to an upper Hessenberg form followed by a standard QR algorithm. The accuracy of the scheme was confirmed by increasing N and the periodicity interval L.

A point to be noted is that infinite-domain eigenvalue problems like (23*a*) can also be solved with the Evans function method. The key element of the Evans function theory, which was introduced by Evans (1972) in his study on nerve impulse stability in relation to the Hodgin–Huxley nerve axon equations, is to define the discrete eigenvalues as the zeros of an analytic function of λ, the Evans function. In our case, there is a four-dimensional set of solutions associated with $\hat{h}$ (recall that there are four spatial eigenvalues for a given λ – see (25*a*)). The eigenvectors (of the dynamical system (23*a*) for $\boldsymbol{\phi}$, $\boldsymbol{\phi}_x$, $\boldsymbol{\phi}_{xx}$, $\boldsymbol{\phi}_{xxx}$) with $\boldsymbol{\phi}$ the eigenfunction $[\hat{h}, \hat{T}]^t$) associated with the spatial eigenvalues with negative real parts form a basis for the subspace of solutions that approach zero as $x \to \infty$, while the eigenvectors associated with the spatial eigenvalues with positive real parts form a basis for the subspace of solutions that approach zero as $x \to -\infty$. Then λ is an eigenvalue if the two subspaces have a non-trivial intersection. That is, we need a condition for the intersection of two linear subspaces of functions. The condition is that the Evans function, defined to be the Wronskian of the basis functions of the two subspaces, should vanish. This is effectively a solvability condition. In our numerical scheme a solvability condition

must also be satisfied (see (29)) and in that sense the global Fourier spectral expansion employed here for the solution of the eigenvalue problem can be viewed as an implicit representation of the Evans function method.

A number of authors have constructed spectra of infinite-domain eigenvalue problems. For example Chang, Demekhin & Kopelevich (1996) and Chang, Demekhin & Kalaidin (1998) obtained the spectrum that governs the stability of pulse solutions of the generalized Kuramoto–Sivashinsky equation. Chang & Demekhin (1999) examined the spectrum of solitary waves on a thin film falling down a vertical fibre while Ye & Chang (1999) investigated the discrete/essential spectrum for the driven contact line problem down a prewetted plane. More recently Kalliadasis & Homsy (2001) considered the spectrum of the infinite-domain eigenvalue problem that determines the stability of free-surface thin film flows over topography. In all these studies (the spectra were defined and constructed using the Evans function method) the essential spectrum has been associated with the flat-film Fourier modes. This observation deserves special attention. In our case, if the base state is a flat film of unit thickness the spectrum will consist of the continuum of Fourier modes $e^{\lambda t+i\alpha x+i\beta z}$ with the dispersion relationship

$$\lambda = -3i\alpha - \frac{Re\,We}{3}(\alpha^2+\beta^2)^2,$$

which is exactly the locus of the essential spectrum Γ_1 in (26a). The reason is simply that the free-surface bump in figure 2 decays to the flat film at both infinities and the oscillations of the eigenfunctions must also be described by the flat-film dispersion relationship (however, the normal modes of the flat film $h = 1$ are modified in the vicinity of $x = 0$ due to the presence of the bump). Since $\lambda_R < 0$, the flat-film regions of thickness 1 are stable. Indeed, as has been shown by Benjamin (1957) a thin flat film can only be destabilized with small but finite inertia. From the dispersion relation above we also obtain $\lambda_I = -3\alpha$. Thus the normal modes on the flat-film regions represent monochromatic infinitesimal disturbances that travel steadily with the kinematic wave velocity $-\lambda_I/3$. As λ_I is a linear function of α, the regions $h = 1$ away from the free-surface bump in figure 2 are also non-dispersive. Thus, any localized disturbances away from the bump will not spread but will propagate at the phase velocity 3 and at the same time decay at the rate λ_R.

Typical computations of both the essential and discrete spectrum are shown in figure 5(a) for $\beta = 0$. Here we used $N = 200$ for the Fourier expansion in (28). The crosses and stars are the eigenvalues of $\boldsymbol{A}$. As $N \to \infty$ and $\delta \to 0$ the distance between the crosses tends to zero and this part of the matrix spectrum tends to the essential spectrum of $\mathscr{L}$. The mode indicated with a star is the only eigenvalue which is not affected by increasing N and decreasing δ (provided of course that N is sufficiently large and δ sufficiently small). This real mode represents a discrete mode of $\mathscr{L}$ (a second real discrete mode at large negative values not shown in the figure is also present). Figure 5(b) shows the computed essential/discrete spectrum for $\beta = 0.02$. Now the branch Γ_1 of the essential spectrum has moved to the left (recall that Γ_2 is independent of β) and there is an additional discrete real mode on the positive real axis – the large negative discrete mode has now moved to $-\infty$.

The generation of this second discrete mode is related to the existence of a 'resonance pole'. Such resonance poles appear in quantum scattering theory (Reed & Simon 1978) and they have been associated with the so-called 'Landau damping' in the Vlasov–Poisson system (Crawford & Hislop 1989). Resonance poles have also been found in stability studies of solitary pulses of the generalized Kuramoto–Sivashinsky

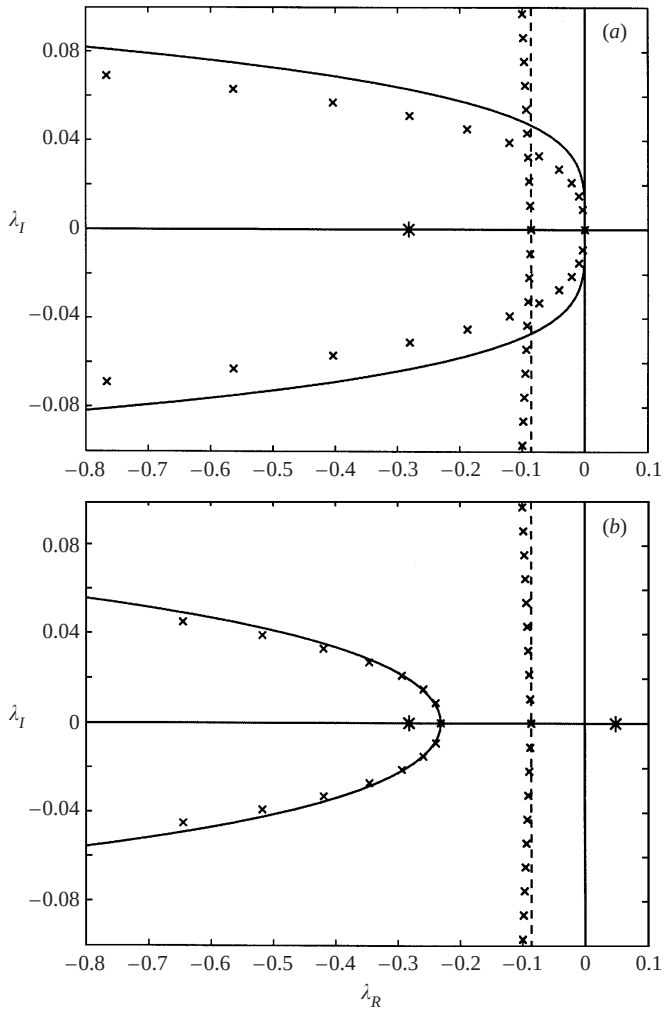

FIGURE 5. Typical essential and discrete spectra of $\mathscr{L}$ for the parameter values in figure 4 and $Ma = 60$. The dashed line is the branch Γ_2 of the essential spectrum obtained from (26*b*). Crosses and stars are the eigenvalues of $\boldsymbol{A}$ corresponding to the essential and discrete spectrum respectively. Also shown is the branch Γ_1 of the essential spectrum obtained from (26*a*). (*a*) $\beta = 0$, one discrete mode; (*b*) $\beta = 0.02$, two discrete modes.

equation (Chang *et al.* 1996, 1998). We note that the corresponding 'eigenfunctions' of resonance poles have unbounded (exponential) growth at one of the infinities and hence resonance poles are not true eigenvalues. However, as β varies, a resonance pole can cross the essential spectrum and become a true discrete eigenvalue, and vice versa. In figure 5(*a*), a resonance pole between a discrete mode and the origin of the spectral plane crosses Γ_1 as β increases and gives birth to a discrete eigenvalue. As the 'eigenfunctions' of resonance poles have unbounded growth at one of the infinities, they cannot be captured by our global Fourier spectral expansion. We shall describe below a modified numerical scheme to locate resonance poles.

Figure 6 shows the generation and destruction of discrete eigenvalues to form resonance poles (and vice versa) at the branch Γ_1 of the essential spectrum (this transition always happens on Γ_1) for the parameter values in figure 4 and $Ma = 10$.

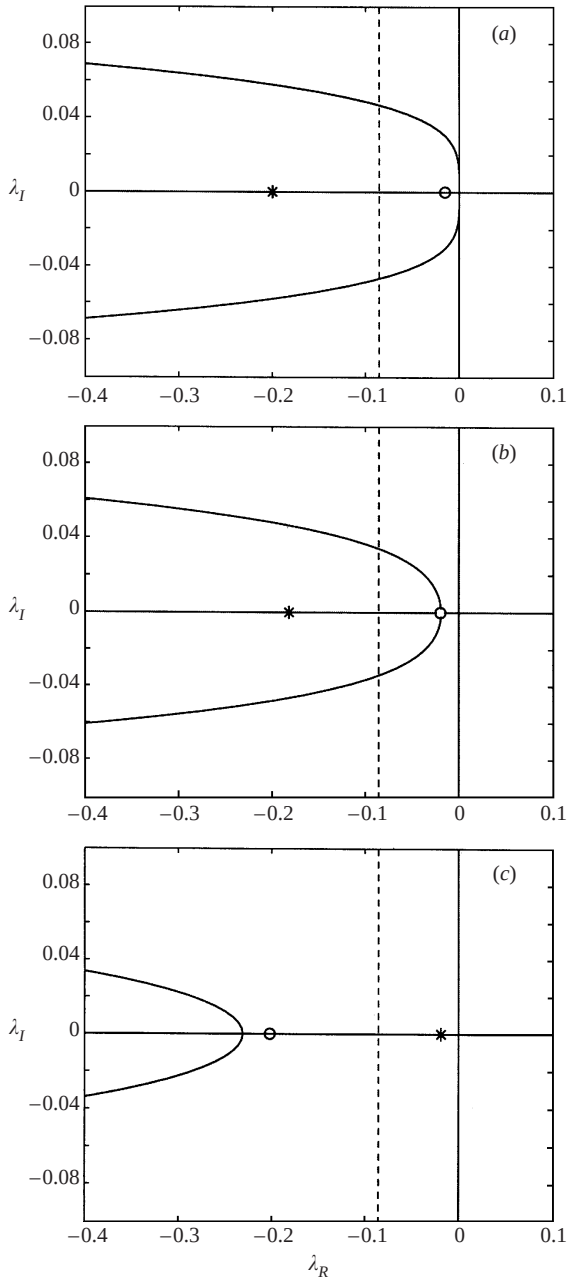

FIGURE 6. Structure of the spectrum for the parameter values in figure 4 and $Ma = 10$. The dashed line indicates the branch Γ_2 of the essential spectrum. The star corresponds to a discrete mode and the open circle to a resonance pole. (*a*) $\beta = 0$, (*b*) $\beta = 0.0107$, (*c*) $\beta = 0.02$.

At $\beta = 0$ the branch Γ_2 of the essential spectrum goes through the origin with a resonance pole (open circle) located on the λ_R-axis between Γ_1 and Γ_2. As β increases branch Γ_1 of the essential spectrum moves to the left of the spectral plane and at $\beta = 0.0107$ the resonance pole is embedded in the essential spectrum. For larger values of β this resonance pole becomes a discrete eigenvalue while the original

discrete mode in figure 6(*a*, *b*) crosses Γ_1, as Γ_1 moves to the left, and becomes a resonance pole. Hence there are two possible transitions: either a resonance pole to the left of Γ_1 becomes a discrete mode to the right or a discrete mode to the left of Γ_1 becomes a resonance pole to the left. The creation/destruction of a discrete mode is related to the essential eigenfunction for $\alpha = 0$ on Γ_1. Recall that Γ_1 is parameterized by the wavenumber α of oscillations of the continuous eigenfunctions as $\alpha \pm \infty$. As $\alpha \to 0$ the essential modes on Γ_1 approach the λ_R-axis and the wavelength of the oscillations becomes infinitely large. As a result this limiting eigenfunction for $\alpha = 0$ approaches constants, say $c_{\pm}$, as $x \to \pm\infty$. Notice that all essential modes for $\alpha \neq 0$ are complex except for the limiting eigenfunction at $\alpha = 0$, which is real.

Consider the case of a resonance pole to the left of Γ_1 becoming a discrete mode to the right. As β approaches a certain value, say β_1, $c_+ \to 0$ and the discrete mode generated at β_1 has the same shape as the continuous mode at this point but approaches zero very slowly as $x \to -\infty$. At the same time, as $\beta \to \beta_1$, the resonance pole has the same shape as the continous mode for $\alpha = 0$ but it blows up slowly towards large positive values as $x \to -\infty$. As β deviates from β_1 the width of the discrete mode decreases rapidly. Now consider the case of a discrete mode to the left of Γ_1 becoming a resonance pole to the right. As β approaches a certain value, say β_2, $c_- \to 0$ and the discrete mode has the same shape as the continuous eigenfunction for $\alpha = 0$ but approaches zero very slowly as $x \to +\infty$. The resonance pole generated at β_2 also has the same shape as the continous eigenfunction for $\alpha = 0$ but blows up slowly towards large positive values as $x \to +\infty$.

Following Pego & Weinstein (1992) and Reed & Simon (1978) the locus of the essential spectrum can be considered as a branch cut that separates two Riemann sheets of the Evans function: one Riemann surface has the resonance poles to the left of Γ_1 with the discrete modes to the right and the other Riemann surface has the discrete modes to the left of Γ_1 with the resonance poles to the right. The eigenvalues which cross Γ_1 to become resonance poles effectively move from one Riemann sheet to the other (this type of bifurcation is rather unusual for eigenvalue problems in a finite domain). To locate these resonance poles we have to suppress their growing tails at the infinities. Pego & Weinstein (1992) pointed out that resonance poles can be regarded as true eigenvalues of an appropriately weighted space. Pego & Weinstein (1994) suggested that if one places a weight that decays exponentially in the direction of unbounded growth for the resonance pole, this growth can be *filtered* away. Hence, we place a spatial filter $e^{\xi x}$ with ξ an arbitrary real number larger than the more negative real part of the spatial eigenvalues as $x \to -\infty$ and smaller than the largest positive real part of the spatial eigenvalues as $x \to +\infty$ (as this spatial mode with the largest positive real part has been suppressed, $e^{\xi x}$ will also be suppressed as $x \to +\infty$). Hence, we introduce the weighted eigenfunctions

$$\hat{\psi}(x) = e^{\xi x}\hat{h}(x), \tag{30a}$$

$$\hat{\theta}(x) = e^{\xi x}\hat{T}(x). \tag{30b}$$

The new eigenvalue problem now has the form

$$\mathscr{L}_\xi \begin{bmatrix} \hat{\psi} \\ \hat{\theta} \end{bmatrix} + \lambda \begin{bmatrix} \hat{\psi} \\ \hat{\theta} \end{bmatrix} = 0 \tag{31}$$

where the operator $\mathscr{L}$ in (23*a*) is transformed to the weighted operator

$$\mathscr{L}_\xi = e^{\xi x}\mathscr{L}\, e^{-\xi x}.$$

This eigenvalue problem is numerically solved with the global Fourier spectral expansion used for the original eigenvalue problem in (23*a*). It is clear that the branch $\Gamma_{1\xi}$ of the essential spectrum of $\mathscr{L}_\xi$ is defined by shifting Γ_1 of $\mathscr{L}$ by the transformation $\alpha \to \alpha + \mathrm{i}\xi$,

$$\lambda = -3i(\alpha + \mathrm{i}\xi) - \frac{Re\,We}{3}[(\alpha + \mathrm{i}\xi)^2 + \beta^2]^2. \tag{32}$$

The second branch of the essential spectrum is also shifted in the same way.

Resonance poles will have a direct influence on the time-dependent behaviour of the system. Stable resonance poles, for example, are responsible for determining the decay rate and drainage dynamics of excited solitary pulses when excess mass is added to equilibrium pulses (Chang *et al.* 1996, 1998; Chang & Demekhin 1999). This mass is carried by localized disturbances on the flat-film regions which generate expanding radiation wave packets that threaten to engulf the pulse unless the pulse outruns or is outrun by the expanding growing wave packet. Hence, such eigenmodes can be used to describe the transient dynamics between stable solitary pulses and radiation modes and have been intimately related to convective stability of solitary pulses. For our problem, the influence of resonance poles can be seen in non-stationary time-dependent computations when a mass of liquid is added at the front or back of the free-surface ridge in figure 2, depending on the direction of the growing tail: for instance, when a discrete mode crosses the essential spectrum from the right of the essential spectrum to become a resonance pole to the left, the exponentially growing tail occurs as $x \to -\infty$. Such time-dependent computations are beyond the scope of the present study.

Figures 7 and 8 show the structure of the spectrum for $Ma = 35$ and $Ma = 60$ respectively and the parameter values in figure 6. For $Ma = 35$ the discrete eigenvalue that bifurcates from the resonance pole at $\beta = 0.009$ approaches the imaginary axis of the spectral plane as β increases and is eventually located at the origin of the spectral plane for $\beta = 0.03$. Further increase of β causes this discrete mode to move to the left (not shown). When the Marangoni number is increased above the value of 35, the discrete eigenvalue that bifurcates from the resonance pole becomes unstable for all β larger than 0.006. Notice the existence of two discrete modes for $\beta = 0.02$ in figure 8. Eventually the stable discrete mode will collide with the essential spectrum for larger values of β and will bifurcate into a resonance pole. These computations reveal the existence of a *critical* Marangoni number, $Ma = Ma^*$, above which the base state becomes linearly unstable with respect to disturbances in the spanwise direction. For the parameter values in figures 6–8, $Ma^* = 35$. This observation is consistent with the experimental findings by Kabov *et al.* (1996, 1999), Kabov (1998) and Scheid *et al.* (2000) which clearly indicate that the instability develops at a certain critical value of the heat flux from the solid boundary to the liquid. Notice that in the experiments the heater has a finite size in the transverse direction and as a result, in some cases, the thermocapillary instability starts from the ends of the heater. With a finite heater, it is likely that the end effects will produce a so-called 'perturbed' or 'imperfect' bifurcation from the 'perfect' laterally infinite case with the spanwise modes starting from the ends and then filling the domain in the transverse direction. Such finite size effects due to lateral boundary conditions at or near criticality are discussed by Fauve (1998).

Figure 9 depicts the dispersion relation $\lambda = \lambda(\beta)$ for the (dominant) least-stable eigenvalue λ associated with the discrete part of the spectrum. As we have already pointed out there is a critical Marangoni number Ma^* for the onset of the instability.

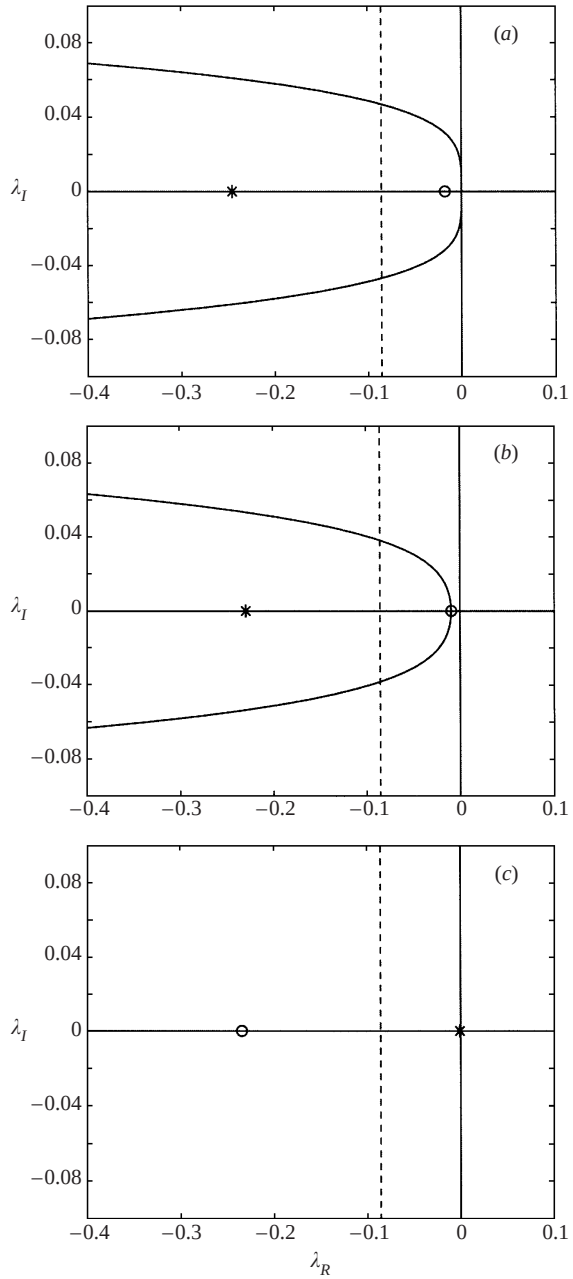

FIGURE 7. As figure 6 but for $Ma = 35$. (*a*) $\beta = 0$, (*b*) $\beta = 0.009$, (*c*) $\beta = 0.03$.

At this Marangoni number, a critical wavenumber, say β_c, becomes unstable first (for the case in figure 9, $\beta_c \simeq 0.03$); at slightly higher values of Ma there is a narrow band of unstable wavenumbers (hence the situation here looks similar to the classical Rayleigh–Bénard convection). For $Ma > Ma^*$ the band of unstable wavenumbers increases and the most amplified eigenmode occurs at wavenumbers larger than β_c. Figure 9(*b*) shows the dispersion relation of figure 9(*a*) in the region of small β. Also shown are the resonance poles (dashed lines) as a function of β and for different

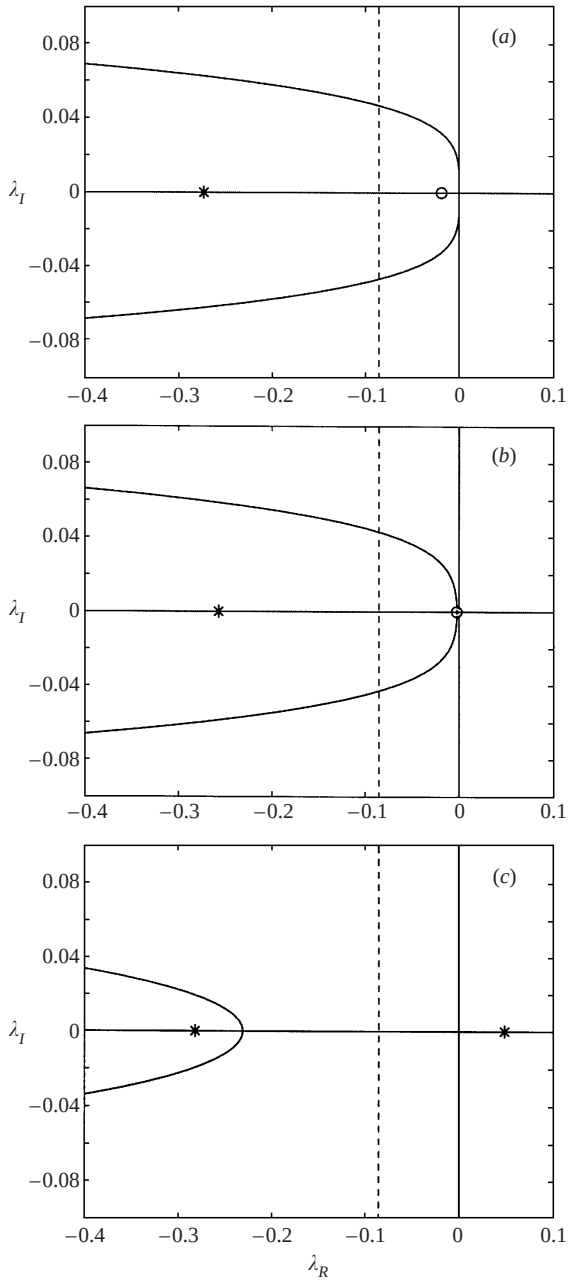

FIGURE 8. As figure 6 but for $Ma = 60$. (*a*) $\beta = 0$, (*b*) $\beta = 0.006$, (*c*) $\beta = 0.02$.

values of the Marangoni number; as we have already pointed out these resonance poles are true discrete modes for the eigenvalue problem (31) but not the original problem (23*a*).

In figure 10 we plot the maximum growth rate, $\lambda_{\max}$, and the maximum growing wavenumber, $\beta_{\max}$, as a function of Marangoni number for the dispersion relation curves in figure 9. Increasing Ma increases $\lambda_{\max}$, making the bump profile in figure 2

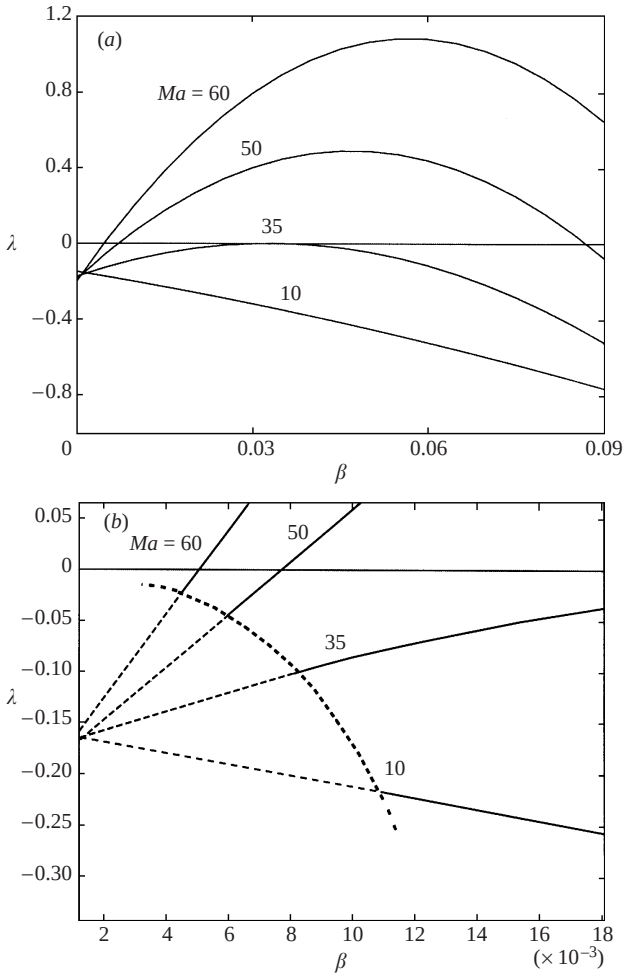

FIGURE 9. (*a*) Dispersion relation, $\lambda = \lambda(\beta)$, for the discrete part of the spectrum as a function of Marangoni number. All parameter values are the same as figure 4. (*b*) Dispersion relation for the discrete part of the spectrum in the region of small wavenumbers. The dashed lines correspond to resonance poles which eventually bifurcate to discrete eigenvalues.

more unstable. At the same time, increasing Ma results in decreasing the wavelength, say $L_{\max}$ $(= 2\pi/\beta_{\max})$, of the rivulets developed in the spanwise direction.

Let us now convert our predictions for the instability wavelength to dimensional quantities. In the absence of experimental values for Biot numbers of liquid–gas interfaces we take $Bi = 1$ (as in all our figures) and we refrain from a quantitative comparison with the experiments by Kabov *et al.* (1996, 1999), Kabov (1998) and Scheid *et al.* (2000). We notice, however, that our definition of the Biot number in (7), $Bi = \alpha h_0/k$ with α the heat transfer coefficient at the free surface, h_0 the film thickness away from the bump and k the thermal conductivity of the liquid phase, implies that the (dimensionless) Biot number is proportional to the film thickness h_0 with the proportionality coefficient α/k a function of the fluid properties. This dependence on h_0 was made explicit by Goussis & Kelly (1991) in their study of the thermocapillary instability of a flat film on a uniformly heated inclined plane. In terms of the variables

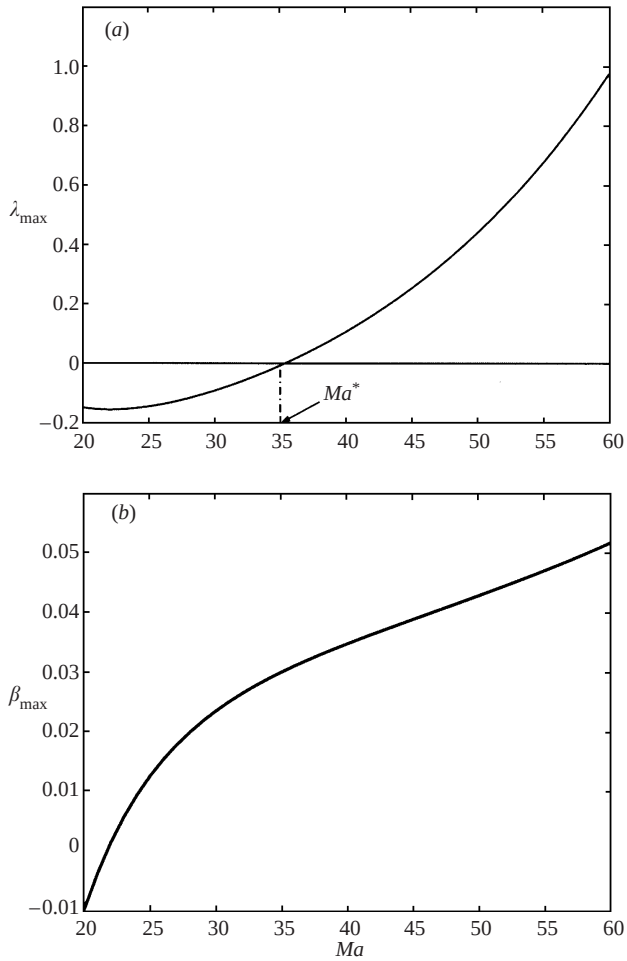

FIGURE 10. (*a*) Maximum growth rate, $\lambda_{\max}$, and (*b*) maximum growing wavenumber, $\beta_{\max}$, as a function of Marangoni number for the dispersion relation curves in figure 9.

used here, Goussis & Kelly define the Biot number as $Bi' = (\alpha/k)(3v^2/g\sin\theta)^{1/3}$ such that $Bi = Bi'Re^{1/3}$ with Bi' depending on the physical properties of the fluid only (like the Kapitza number γ). Hence, changing h_0, or equivalently the Reynolds number, implies changing the Biot number.

For water at 25°, $\kappa = 5\times10^{-5}\,\mathrm{kg\,s^{-2}\,K^{-1}}$, $k = 0.607\,\mathrm{W\,m^{-1}\,K^{-1}}$, $c_P = 4.18\,\mathrm{J\,g^{-1}\,K^{-1}}$, $\mu = 10^{-2}\,\mathrm{g\,cm^{-1}\,s^{-1}}$, $\rho = 1\,\mathrm{g\,cm^{-3}}$ and $\sigma = 61\,\mathrm{dyn\,cm^{-1}}$ (see for example Reid, Prausnitz & Sherwood 1977). This gives $Pr \simeq 7$ which is the value used in all our figures. With $Re = 1$, the film thickness away from the bump can be computed from $h_0 = (3v^2Re/g\sin\theta)^{1/3}$ (see the definition of Reynolds number in (3*a*)) which with $\theta = \pi/2$ gives $h_0 = 0.067\,\mathrm{mm}$. From the definition of Marangoni number in (6) and for a temperature difference $\Delta T = 10\,\mathrm{K}$, well within an achievable range, we obtain $Ma \simeq 35$ which is the critical Marangoni number shown in figures 9 and 10 (any ΔT less than 10 K will not induce an instability). From figure 10(*b*), $\beta_{\max} \simeq 0.03$ and hence the dimensional wavelength for the instability in the transverse direction is $\tilde{L}_{\max} = (2\pi/\beta_{\max})h_0 \simeq 14\,\mathrm{mm}$.

Pr	Ma^*	$\beta^*_{\max}$
0.1	31.012	0.028
5.0	31.707	0.0281
7.0	35.02	0.03
10.0	38.18	0.033
20.0	57.101	0.051

TABLE 1. Variation of critical Marangoni number, Ma^*, and maximum growing wavenumber at criticality, $\beta^*_{\max}$, as a function of Pr for $\gamma = 2850$, $\theta = \pi/2$ and $Re = Bi = 1$.

Table 1 gives the variation of the critical Marangoni number, Ma^*, and maximum growing wavenumber, $\beta^*_{\max}$, as a function of Prandtl number for $\gamma = 2850$, $Re = 1$ and $Bi = 1$. As Pr (or equivalently $Pe = Pr\,Re$) decreases, the critical Marangoni number decreases which means that the system can be destabilized more easily. This is due to large temperatures on the free surface – at very small Pe the free-surface temperature distribution is not convected downstream (a simple comparison of the temperature profile in figure 3 with the distribution in (16) shows that indeed T_s in figure 3 is smaller than T_s from (16)). Hence, the instability persists in the region of small Péclet numbers where the temperature distribution on the free surface is adiabatically slaved to the film thickness. The limiting critical Marangoni number as $Pr \to 0$ for $Re = Bi = 1$ is $Ma^* \simeq 31$.

For a 25% by mass mixture of ethanol in water used in the experiments by Kabov *et al.* (1996), $\kappa = 0.11 \times 10^{-3}\,\mathrm{kg\,s^{-2}\,K^{-1}}$, $k = 0.438\,\mathrm{W\,m^{-1}\,K^{-1}}$, $c_P = 3.745\,\mathrm{J\,g^{-1}\,K^{-1}}$, $\mu = 1.94 \times 10^{-2}\,\mathrm{g\,cm^{-1}\,s^{-1}}$, $\rho = 0.95\,\mathrm{g\,cm^{-3}}$ and $\sigma = 34.53\,\mathrm{dyn\,cm^{-1}}$ (see Reid *et al.* 1977 on how to estimate properties of aqueous solutions). These values give $\gamma \simeq 655$ and $Pr \simeq 17$. We can now use our computations in figures 9, 10 and table 1 to obtain the instability wavelength for this liquid. As already mentioned, although these computations are for water which has $\gamma = 2850$, they are valid for all cases with $We\,Re = 4110$ – recall that the governing dimensionless groups are $We\,Re$ (both Weber and Reynolds numbers appear always as a product), Ma, Pe and Bi. Similarly, table 1 gives the variation of Ma^* and $\beta^*_{\max}$ as a function of Péclet number (Pr appears always as a product with the Reynolds number). Hence, the results of figures 9, 10 are valid for $3^{1/3}\gamma/Re^{2/3} = 4110$, $Pe = 7$ with $\theta = \pi/2$ while the results in table 1 are valid for $3^{1/3}\gamma/Re^{2/3} = 4110$ and different Péclet numbers. From $3^{1/3}\gamma/Re^{2/3} = 4110$ and $\gamma = 655$ we obtain $Re = 0.11$. From the definition of Reynolds number in (3*a*) then we obtain $h_0 = 0.05\,\mathrm{mm}$. Table 1 shows that the critical Marangoni number for $Pe = Re\,Pr \simeq 1.87$ is $Ma^* \simeq 31$ which from the definition of Marangoni number in (6) gives $\Delta T \simeq 2\,\mathrm{K}$ – any temperature difference less than this value will not induce instability. From table 1 we also obtain the maximum growing wavenumber at criticality, $\beta^*_{\max} \simeq 0.028$. The instability wavelength is then $\tilde{L}_{\max} = 2\pi/\beta^*_{\max} h_0 \simeq 11\,\mathrm{mm}$, of the same order of magnitude as the value of $\simeq 6\,\mathrm{mm}$ for $Re = 0.4$ obtained in the experiments by Kabov *et al.* (1996). The agreement becomes much better if we assume a larger ΔT, for example temperature differences as large as 10 K or even larger were observed in the experiments. With $\Delta T = 10\,\mathrm{K}$, we obtain $Ma \simeq 140$. With this value of Marangoni number and with $Pe \simeq 1.87$ the solution of the eigenvalue problem gives $\beta^*_{\max} \simeq 0.065$ which in turn gives $\tilde{L}_{\max} \simeq 5\,\mathrm{mm}$.

Notice that in the experiments a constant flux is imposed at the solid boundary

instead of specifying a temperature distribution as we did here. The IBL treatment of a constant flux condition is more involved and the final equations more complicated than (13*a–d*). But even with a flux boundary condition on the wall, we cannot have a quantitative comparison with the experiments since, as already emphasized, the heat transfer coefficient and therefore the Biot number is not known. For this reason, comparisons with experiments for free-surface thermocapillary flows are mainly qualitative (see Nepomnyashchy *et al.* 2001). As the Biot number is unknown, different authors assume different values for this dimensionless group. For instance, the heat transfer coefficient used by Scheid *et al.* (2001) gives $Bi = 0.1$ which corresponds to $Bi' = 0.13$ – recall that this is the Goussis & Kelly (1991) definition of the Biot number. Goussis & Kelly in their study of the linear stability of a film falling down a uniformly heated plane chose the value $Bi' = 10$. The same value was recently adopted by Kalliadasis, Demekhin & Velarde (2002) in their study of the nonlinear instability of the Goussis & Kelly problem.

5. Summary

We have considered the thermocapillary instability of a falling liquid film heated from below by a heating device on the substrate. The transverse dimension of the heater is much longer than its width in the streamwise direction. The heating generates a temperature distribution on the free surface which induces surface tension gradients that drive the fluid away from the heated region. This thermocapillary flow was modelled by using the IBL approximation of the Navier–Stokes/energy equations and free-surface boundary conditions. The IBL approximation results in a system of two coupled partial differential equations for the evolution of the local film height and free-surface temperature distribution in time and space.

Two-dimensional steady states of these equations are reported for a Gaussian temperature distribution on the wall and different values of the Marangoni number. In all cases, the free surface develops a bump in the region where the wall temperature gradient is positive. The height of this bump was found to be an increasing function of the Marangoni number. In addition, we computed the temperature distribution on the free surface and demonstrated that for finite Péclet numbers the temperature field is convected downstream resulting in a free-surface temperature distribution with a maximum in the region where the wall temperature gradient is negative.

We then analysed the linear stability of the steady states with respect to disturbances in the spanwise direction. The stability problem was formulated in a way that allowed for disturbances that did not necessarily decay at the infinities. In this way, we were able to analyse the complete spectrum of the resulting linear eigenvalue problem, which proved to be particularly subtle in its structure. We found that the operator of the linearized system has both a discrete and an essential spectrum. The discrete spectrum consists of eigenfunctions localized around the base state while the essential spectrum consists of eigenfunctions which approach bounded oscillations at the infinities – the essential spectrum is described by the dispersion relationship of the flat films away from the bump and hence it is always stable.

For a given Marangoni number, the discrete spectrum only exists for disturbances with wavenumber above a critical value. At this value, a resonance pole, with a corresponding eigenfunction that has unbounded growth at one of the infinities, crosses the essential spectrum and becomes a discrete eigenvalue. Hence, the discrete spectrum is born out of resonance poles at specific values of the wavenumber for the disturbances in the spanwise direction.

Our main result is that, for small values of the Marangoni number, the discrete spectrum is always stable, while at a critical Marangoni number a discrete mode becomes unstable and for values of the Marangoni number larger than this critical value, there is a band of unstable discrete modes. We have computed the critical Marangoni number and the maximum growing wavenumber at criticality as a function of Péclet number and showed that small Péclet numbers decrease the critical Marangoni number and hence destabilize the system more easily. Finally, we attempted to compare our theoretical predictions with available experimental data. However, the absence of experimental values for heat transfer coefficients at liquid–gas interfaces have prevented us from a quantitative comparison with the experiments.

There are a number of interesting questions related to the analysis presented here and our theory can be extended in several directions. For example, it would be interesting to compare the IBL approximation for the energy equation developed here to Benney's equation with the temperature distribution given by (16) adopted by Joo *et al.* (1991) and Scheid *et al.* (2001). Preliminary analysis by Kalliadasis *et al.* (2002) indicates that Benney's equation gives unrealistic solutions, including finite-time blow-up behaviour, in certain regimes of the parameter space. The same authors have also scrutinized the validity of the linear approximation in (12) and demonstrated that the linear stability of the flat-film solution with this temperature distribution is in good agreement with the Orr–Sommerfeld stability analysis of the full energy equation. The agreement becomes better when (12) is replaced with a parabolic temperature distribution (in which case of course equation (13*d*) for the free-surface temperature distribution is more complex). Another related problem is the IBL treatment of a constant-heat-flux boundary condition at $y = 0$ instead of specifying the temperature distribution at $y = 0$. In this case the weight function of (2*c*) is simply 1 but the final equations are more complicated than the system (13*a–d*). Of particular interest would also be a detailed examination of the effects of inertia on the thermocapillary instability. For this purpose, we would have to use the full IBL equations (13*a*, *b*) instead of their simplified versions (14*a*, *b*) which assume that the flow rates q and p are slaved to the film thickness h. Other related issues include three-dimensional numerical simulations of the full IBL equations (13*a–d*) for the nonlinear stage of the thermocapillary instability and the development of a systematic approach to obtain the Biot number as a function of the other dimensionless groups, including a possible dependence on x (such a dependence was pointed out by Kabov *et al.* (1996); preliminary analysis assuming a fully developed laminar boundary layer in the gas phase indicates that Bi is a decreasing function of x). This and other problems will be addressed in a future paper.

S. K. is grateful to Professor V. V. Pukhnachev for introducing him to the problem and Professor G. M. Homsy for helpful comments and stimulating discussions on Marangoni effects and heat transport at finite Péclet numbers. E. A. D. thanks the Chemical Engineering Department at Leeds University for hospitality and acknowledges financial support from the Engineering and Physical Sciences Research Council of England, through a Visiting Fellowship, grant no. GR/R61772/01.

Appendix. The coefficients of the eigenvalue problem

The coefficients S_i and G_i in (24) depend on the base-state solution of (17a, b) and are parameterized by the spanwise wavenumber β:

$$G_1 = \frac{7}{40}\frac{T_s - f}{h}E_1, \quad G_2 = \frac{7}{40}\frac{T_s - f}{h}E_1' + \left(\frac{21}{40}\frac{f'}{h} + \frac{27}{20}\frac{T_s'}{h}\right)E_1,$$

$$G_3 = \frac{7}{40}\frac{T_s - f}{h}E_2 + \frac{7}{40}\frac{T_s - f}{h}\mathrm{i}\beta E_5, \quad G_4 = \frac{7}{40}\frac{T_s - f}{h}(E_3 + E_2') + \left(\frac{21}{40}\frac{f'}{h} + \frac{27}{20}\frac{T_s'}{h}\right)E_2,$$

$$G_5 = \frac{7}{40}\frac{T_s - f}{h}E_3' + \frac{7}{40}\frac{T_s - f}{h}\mathrm{i}\beta E_6 + \left(\frac{21}{40}\frac{f'}{h} + \frac{27}{20}\frac{T_s'}{h}\right)E_3$$
$$-\frac{21}{40}\frac{f'}{h^2} - \frac{27}{20}\frac{T_s'}{h^2} + \frac{3}{Pe}\left[-\frac{BiT_s}{h^2} + 2\frac{f - T_s}{h^3}\right],$$

$$G_6 = \frac{7}{40}\frac{T_s - f}{h}E_4, \quad G_7 = \frac{7}{40}\frac{T_s - f}{h}E_4' + \left(\frac{21}{40}\frac{f'}{h} + \frac{27}{20}\frac{T_s'}{h}\right)E_4 + \frac{27}{20}\frac{1}{h},$$

$$G_8 = \frac{7}{40}\frac{T_s - f}{h}\mathrm{i}\beta E_7 + \frac{3}{Pe}(Bi + 1)\frac{1}{h};$$

$$S_1 = E_1, \quad S_2 = E_1', \quad S_3 = E_2 + \mathrm{i}\beta E_5, \quad S_4 = E_3 + E_2',$$

$$S_5 = E_3' + \mathrm{i}\beta E_6, \quad S_6 = E_4, \quad S_7 = E_4', \quad S_8 = \mathrm{i}\beta E_7,$$

where the prime denotes differentiation with respect to x and

$$E_1 = \frac{Re\,We}{3}h^3, \quad E_2 = -\frac{Re\,We}{3}\beta^2 h^3 - \cot\theta h^3,$$

$$E_3 = 3h^2 - 3h^2 h' \cot\theta + Re\,We\,h^2 h''' + Ma\,hT_s',$$

$$E_4 = \tfrac{1}{2}Ma\,h^2, \quad E_5 = \mathrm{i}\beta\frac{Re\,We}{3}h^3, \quad E_6 = -\mathrm{i}\beta^3\frac{Re\,We}{3}h^3, \quad E_7 = -\tfrac{1}{2}\mathrm{i}\beta Ma\,h^2.$$

REFERENCES

Alekseenko, S. V., Nakoryakov, V. E. & Pokusaev, B. G. 1994 *Wave Flow of Liquid Films*. Begel House.

Ames, W. F. 1977 *Numerical Methods for Partial Differential Equations*. Academic.

Bankoff, S. G. 1994 Significant questions in thin liquid film heat transfer. *Trans. ASME: J. Heat Transfer* **116**, 10–16.

Benjamin, T. B. 1957 Wave formation in laminar flow down an inclined plane. *J. Fluid Mech.* **2**, 554–574.

Benney, B. J. 1966 Long waves in liquid films. *J. Math. Phys.* **45**, 150–155.

Bertozzi, A. L. & Brenner, M. P. 1997 Linear stability and transient growth in driven contact lines. *Phys. Fluids* **9**, 530–539.

Burelbach, J. B., Bankoff, S. G. & Davis, S. H. 1988 Nonlinear stability of evaporating/condensing liquid films. *J. Fluid Mech.* **195**, 463–494.

Chang, H.-C. 1994 Wave evolution on a falling film. *Annu. Rev. Fluid Mech.* **26**, 103–136.

Chang, H.-C. & Demekhin, E. A. 1999 Mechanism for drop formation on a coated vertical fibre. *J. Fluid Mech.* **380**, 233–255.

Chang, H.-C., Demekhin, E. A. & Kalaidin, E. 1998 Generation and suppression of radiation by solitary pulses. *SIAM J. Appl. Maths* **58**, 1246–1277.

Chang, H.-C., Demekhin, E. A. & Kopelevich, D. I. 1993 Nonlinear evolution of waves on a vertically falling film. *J. Fluid Mech.* **250**, 433–480.

Chang, H.-C., Demekhin, E. A. & Kopelevich, D. I. 1996 Local stability theory of solitary pulses in an active medium. *Physica* D **97**, 353–375.

Crawford, J. D. & Hislop, P. D. 1989 Application of the method of spectral deformation to the Vlasov–Poisson system. II. Mathematical results. *J. Math. Phys.* **30**, 2819–2837.

Davis, S. H. 1987 Thermocapillary instabilities. *Annu. Rev. Fluid Mech.* **19**, 403–435.

Demekhin, E. A. & Schkadov, V. Ya. 1984 Three-dimensional waves in a liquid flowing down a wall. *Izv. Akad. Nauk SSSR, Mekh. Zhidk Gaza* **5**, 21–27.

Demekhin, E. A. & Velarde, M. G. 2001 Suppressing surface and convective instabilities by Marangoni forces. *Phys. Fluids* (submitted for publication).

Evans, J. W. 1972 Nerve axon equations: 1 Linear approximations. *Indiana Univ. Math. J.* **21**, 877–885.

Fauve, S. 1998 Pattern forming instabilities. *Hydrodynamics and Nonlinear Instabilities* (ed. C. Godrèche & P. Manneville). Cambridge University Press.

Goodwin, R. & Homsy, G. M. 1991 Viscous flow down a slope in the vicinity of a contact line. *Phys. Fluids* **3**, 515–528.

Goussis, D. A. & Kelly, R. E. 1991 Surface wave and thermocapillary instabilities in a liquid film flow. *J. Fluid Mech.* **223**, 25–45.

Gramlich, C. M., Kalliadasis, S., Homsy, G. M. & Messer, C. 2002 Optimal leveling over one-dimensional topography by Marangoni stresses. *Phys. Fluids* **14**, 1841–1850.

Joo, S. W., Davis, S. H. & Bankoff, S. G. 1991 Long-wave instabilities of heated falling films: two-dimensional theory of uniform layers. *J. Fluid Mech.* **230**, 117–146.

Kabov, O. A. 1998 Formation of regular structures in a falling liquid film upon local heating. *Thermophys. Aeromech.* **5**, 547–551.

Kabov, O. A., Marchuk, I. V. & Chupin, V. M. 1996 Thermal imaging study of the liquid film flowing on a vertical surface with local heat source. *Russ. J. Engng Thermophys.* **6**, 105–138.

Kabov, O. A., Marchuk, I. V., Muzykantov, A. V., Legros, J. C., Istasse, E. & Dewandel, J. L. 1999 Regular structures in locally heated falling liquid films. In *Proc. 2nd Intl Symp. on Two-phase Flow Modelling and Experimentation* (ed. G. P. Celata, P. DiMarco & R. K. Shah), Pisa.

Kalliadasis, S. 2000 Nonlinear instability of a contact line driven by gravity. *J. Fluid Mech.* **413**, 355–378.

Kalliadasis, S., Demekhin, E. A. & Velarde, M. G. 2002 Thermocapillary instability and wave formation on a film falling down a uniformly heated plane. *J. Fluid Mech.* (submitted for publication).

Kalliadasis, S. & Homsy, G. M. 2001 Stability of free-surface thin film flows over topography. *J. Fluid Mech.* **448**, 387–410.

Kondic, L. & Bertozzi, A. L. 1999 Nonlinear dynamics and transient growth of driven contact lines. *Phys. Fluids* **11**, 3560–3562.

Marchuk, I. V. & Kabov, O. A. 1998 Numerical modeling of thermocapillary reverse flow in thin liquid films under local heating. *Russ. J. Engng Thermophys.* **8**, 17–46.

Nakaya, C. 1975 Long waves on a thin fluid layer flowing down an inclined plane. *Phys. Fluids* **18**, 1407–1412.

Nepomnyashchy, A. A., Velarde, M. G. & Colinet, P. 2001 *Interfacial Phenomena and Convection.* Chapman & Hall.

Oron, A. 1999 Nonlinear dynamics of thin evaporating liquid films subject to internal heat generation. In *Fluid Dynamics at Interfaces* (ed. W. Shyy & R. Narayanan). Cambridge University Press.

Oron, A., Davis, S. H. & Bankoff, S. G. 1997 Long-scale evolution of thin liquid films. *Rev. Mod. Phys.* **69**, 931–980.

Oron, A. & Gottlieb, O. 2002 Nonlinear dynamics of temporally excited falling liquid films. *Phys. Fluids* **14**, 2622–2636.

Oron, A. & Peles, Y. 1998 Stabilization of thin liquid films by internal heat generation. *Phys. Fluids* **10**, 537–539.

Pearson, J. R. A. 1958 On convection cells induced by surface tension. *J. Fluid Mech.* **4**, 489–500.

Pego, R. L. & Weinstein, M. I. 1992 Eigenvalues and instabilities of solitary waves. *Phil. Trans. R. Soc. Lond.* A **340**, 47–94.

Pego, R. L. & Weinstein, M. I. 1994 Asymptotic stability of solitary waves. *Commun. Math. Phys.* **164**, 305–340.

Reed, M. & Simon, B. 1978 *Methods of Modern Mathematical Physics. IV. Analysis of Operators.* Academic.

Reid, R. C., Prausnitz, J. M. & Sherwood, T. K. 1977 *The Properties of Gases and Liquids.* McGraw-Hill.

Rosenau, P., Oron, A. & Hyman, J. M. 1992 Bounded and unbounded patterns of the Benney equation. *Phys. Fluids* A **4**, 1102–1104.

Ruyer-Quil, C. & Manneville, P. 1998 Modelling film flows down inclined planes. *Eur. Phys. J.* B **6**, 277–292.

Ruyer-Quil, C. & Manneville, P. 2000 Improved modelling of flows down inclined planes. *Eur. Phys. J.* B **15**, 357–369.

Ruyer-Quil, C. & Manneville, P. 2002 Further accuracy and convergence results on the modeling of flows down inclined planes by weighted-residual approximations. *Phys. Fluids* **14**, 170–183.

Scheid, B., Kabov, O., Minetti, C., Colinet, P. & Legros, J. C. 2000 Measurement of free surface deformation by reflectance-Schlieren method. In *Proc. 3rd European Thermal Sciences Conf.* (ed. E. W. P. Hahne, W. Heidemann & K. Spindler), Heidelberg.

Scheid, B., Oron, A., Colinet, P., Thiele, U. & Legros, J. C. 2001 Nonlinear evolution of non-uniformly heated falling liquid films. *Phys. Fluids* (submitted for publication).

Schkadov, V. Ya 1967 Wave conditions in the flow of thin layer of a viscous liquid under the action of gravity. *Izv. Akad. Nauk SSSR, Mekh. Zhidk Gaza* **1**, 43–50.

Smith, M. K. & Davis, S. H. 1983*a* Instabilities of dynamic thermocapillary liquid layers. Part 1. Convective instabilities. *J. Fluid Mech.* **132**, 119–144.

Smith, M. K. & Davis, S. H. 1983*b* Instabilities of dynamic thermocapillary liquid layers. Part 2. Surface-wave instabilities. *J. Fluid Mech.* **132**, 145–162.

Spaid, M. A. & Homsy, G. M. 1996 Stability of Newtonian and viscoelastic dynamic contact lines. *Phys. Fluids* **8**, 460–478.

Sternling, C. V. & Scriven, L. E. 1959 Interfacial turbulence: hydrodynamic stability and the Marangoni effect. *AIChE J.* **5**, 514–523.

Troian, S., Herbolzheimer, E., Safran, S. & Joanny, J. 1989 Fingering instabilities of driven spreading films. *Europhys. Lett.* **10**, 25–30.

Ye, Y. & Chang, H.-C. 1999 A spectral theory for fingering on a prewetted plane. *Phys. Fluids* **11**, 2494–2515.